NTNU
Norwegian University of
Science and Technology

MODELLING AND CONTROL OF HORIZONTAL GRAVITY SEPARATOR

Demulsification of Oil-Water Interface

Samuel Emebu

Supervisor: Prof. Sigurd Skogestad

Co-supervisor: Dr. Christoph Backi

JULY 12th, 2018

DEPARTMENT OF CHEMICAL ENGINEERING

Norwegian University of Science and Technology (NTNU)

NTNU
Norwegian University of
Science and Technology

Abstract

In an effort to resolve the underperformance of horizontal gravity separator, a more robust sizing that involves modelling the active separation zone into gaseous phase, oil phase, oil-water interface and water phase. Specially, the influence of oil-water interface or emulsion layer on separation performance is the main aspect of consideration in this work.

The work started off with the use of Stokes law in modelling liquid droplets rising and settling. This is then followed by the development of dynamic models for; pressure of the gas phase, level of the overall liquid phase, level of the oil phase, level of water and oil in emulsion layer, and finally level of water phase in the active separation zone.

Having developed models for the water and oil emulsion layer, performance of the model was then investigated. With the performance validated, the objective of the work proceeded toward defining a model for demulsification of the emulsion layer. A model proposed by Grimes, 2012 to describe the relationship on how interfacial tension, and consequently interaction energy of molecules in emulsion influences coalescence, given in Equation (4.3) -(4.4), was used in modelling the demulsification process.

In applying, Equation (4.3) -(4.4), appropriate values and pairing for interfacial tension, γ, and retarded Hamaker constant, Ha, were deduced to be $(5, 10, 15, 20, 25\ and\ 35 \times 10^{-3}\ N/m\ )$ and $(1.76 \times 10^{-25}, 1.76 \times 10^{-26}, \ldots, 1.76 \times 10^{-30}\ and\ 1.76 \times 10^{-31}\ Jm)$ respectively. These values were used to deduce hypothetically curve fitted relationship between γ and Ha, given in Equation (5.1). subsequently this equation was used to deduce optimal, hypothetical droplet radii, which were found to be approximately $110\mu m$ for water and $90\mu m$ for oil in the emulsion phase.

Having deduced model for demulsification, performance check on the effectiveness of these models were carried out. And with the equations validated, demulsification based controller was then designed for the process. The simulation parameters deduced for well production towards the end of reservoir lifetime are given in Table (8.1), and it was found that these parameters were versatile, as they are also effective in beginning of the reservoir lifetime.

Simulation was then performed using these developed models and various parameter in MATLAB/SIMULINK and Script Files based on two main simulation case studies: Well production in beginning of the reservoir lifetime and towards the end of the reservoir lifetime, with each case simulated for conditions when there is no forced interfacial outflow and when there is forced interfacial outflow.

Preface

This work is a thesis undertaken at the Department of Chemical Engineering, Norwegian University of Science and Technology in Trondheim, Norway. It is compulsory and required to be undertaken by 2nd year Masters' students as a fulfilment of their degree.

This work was undertaken during the spring Semester of 2018 in the Process System Engineering group of the above-mentioned department. This work has afforded me the opportunity to further my desire, in pursuing a research career in Advanced Process Control.

My gratitude goes to God Almighty, for divine strength, direction and provision, thus far in my stay and study.

My gratitude also goes to Professor Sigurd Skogestad, my project supervisor, for providing me the mentorial platform for this project. And also, a heartful thanks to my co-supervisor, Dr. Christoph J. Backi for providing the technical basis, guidance, thoughtful scrutiny and courage throughout the duration of this work.

Declaration of Compliance

I declare that this thesis is an independent work in agreement with the exam regulations of the Norwegian University of Science and Technology (NTNU).

Trondheim, Norway ……

July 12th, 2018 Samuel Emebu

Table of Contents

List of Tables

List of Figures

List of Symbols

Latin Letters

Symbols	Description	Units
L	Active Separation Zone	m
d	Diameter of Separator	m
r	Radius of Separator	m
v	Velocity	m/s
v_c	Velocity of Continuous Phase	m/s
v_{max}	Maximum Velocity	m/s
v_t	Terminal Velocity	m/s
F_D	Drag Force	N
F_B	Buoyancy Force	N
g	Acceleration due to Gravity	m/s^2
D	Droplet Diameter of Dispersed or Liquid Phase	m
D_E	Empirical droplet size	m
D_p	practical droplet sizes	m
P	Pressure of Continuous Phase in Separation Zone	N/m^2 or $Psig$
P_{init}	Initial Pressure	N/m^2 or $Psig$
C_D	Drag Coefficient	$-$
Re	Reynold Number	$-$
N_a	Avogadro's number	$mole^{-1}$
x	Unitless Factor	$-$
k	Proportionality constant of flow Regime	$-$
K_{SB}	Sounder and Brown Design Coefficient	ft/sec
K'_{SB}	Modified K_{SB}	ft/sec
K_{re}	Empirical Correction factor for droplet size	$-$
K_r	Practical Correction factor for droplet size	$-$
K_{flu}	Flushing factor	$-$
K'	Integrating constant	System dependent
K_D	Derivative controller constant	System dependent
K_c	Controller gains for system	System dependent
$e(t)$	Error signal	System dependent
$y_{sp}(t)$	Setpoint	System dependent
$y_m(t)$	Measured Value	System dependent
$P(t)$	Controller output	System dependent
$\bar{P}$	Bias value	System dependent
n_c	Moles of Continuous Phase	$moles$
M_c	Molar Mass of Continuous Phase	$kg/moles$
R	Idea Gas Constant	$m^3 Pa mol^{-1} K^{-1}$
T	Temperature of Fluid	$Kelvins$
Ha	Retarded Hamaker constant	Jm
t_{res}	Residence Time	sec
t_{flu}	Flushing time	sec
t_c	Coalescence time	sec
t_{drop}	Drop Time	sec
t_O	Initial Time of Separation	sec
t	Any Time greater than Initial Time	sec

t_1	Specific Time greater than Initial Time	sec
t_2	Time greater than t_1	sec
h	Hydrostatic Height	m
h_{weir}	Weir height	m
y	Height of Triangular Portion	m
h_C	Height of Continuous Phase in Separation Zone	m
h_O	Initial Height of Oil Phase	m
h_{OC}	Height of Pure Oil Phase	m
h_i	Height of Interface	m
h_{iW}	Height of Water in Interface	m
$h_{iW,init}$	Initial value for the Water interface level	m
h_{iO}	Height of Oil in Interface	m
$h_{iO,init}$	Initial value for the Oil interface level	m
h_L	Height of Liquid	m
$h_{L,init}$	Initial value for the liquid level	m
h_W	Height of Initial Water Phase	m
$h_{W,init}$	Initial value for the water level	m
h_{WC}	Height of Pure Water Phase	m
h_{W+iO}	Height of Water and Oil in Interface	m
h_{G+O}	Height of Gas and Oil	m
h_{G+O+iW}	Height of Gas, Oil and Water in Interface	m
A	Molecular area of the adsorbed demulsifier species	$Å^2$
A_d	Surface Area of a Droplet of Dispersed Phase	m^2
A_O	Area of Initial Oil in Active Separation Zone	m^2
A_{OC}	Area of Pure Oil in Active Separation Zone	m^2
A_i	Area of Interface in Active Separation Zone	m^2
A_W	Area of Initial Water Phase in Active Separation Zone	m^2
A_{WC}	Area of Pure Water Phase in Active Separation Zone	m^2
A_L	Area of Liquid in Active Separation Zone	m^2
A_{iO}	Area of Oil in Interface	m^2
A_{iW}	Area of Water in Interface	m^2
A_{W+iO}	Area of Water and Oil in Interface	m^2
A_{G+O}	Area of Gas and Oil	m^2
A_{G+O+iW}	Area of Gas, Oil and Water in Interface	m^2
V_d	Volume of a Droplet of Dispersed Phase	m^3
V_C	Volume of Continuous Phase in Active Separation Zone	m^3
V_O	Volume of Initial Oil in Active Separation Zone	m^3
V_{OoW}	Volume of Oil out of Water Phase	m^3
V_{OC}	Volume of Pure Oil in Active Separation Zone	m^3
V_W	Volume of Initial Water Phase in Active Separation Zone	m^3
V_{WoO}	Volume of Water out of Oil phase	m^3
V_{WC}	Volume of Pure Water Phase in Active Separation Zone	m^3
V_L	Volume of Liquid in Active Separation Zone	m^3
V_i	Volume of Interface in Active Separation Zone	m^3
V_{iO}	Volume of Oil in interface in Active Separation Zone	m^3
V_{iW}	Volume of Water in interface in Active Separation Zone	m^3
V_{Sep}	Volume of Active Separation Zone	m^3
q_{Gin}	Inlet Volumetric Flowrate of Gas	m^3/s
q_{Lin}	Inlet Volumetric Flowrate of Liquid	m^3/s
q_{Win}	Inlet Volumetric Flowrate of Water	m^3/s
q_{Oin}	Inlet Volumetric Flowrate of Oil	m^3/s

q_{Gout}	Outlet Volumetric Flowrate of Gas	m^3/s
q_{Lout}	Outlet Volumetric Flowrate of Liquid	m^3/s
q_{Wout}	Outlet Volumetric Flowrate of Water	m^3/s
q_{Oout}	Outlet Volumetric Flowrate of Oil	m^3/s
$q_{i,out}$	Interface outflow	m^3/s
$q_{O,out,flu}$	Oil outflow from flushing	m^3/s
Z	Concentration of demulsifier species adsorbed at the interface	mol/m^2

Greek Letters

Symbols	Description	Units
ρ	Density of Fluid	$kg/m^3, lb/ft^3$
ρ_d	Density of Liquid or Dispersed Phase	$kg/m^3, lb/ft^3$
ρ_c	Density of Continuous Phase	$kg/m^3, lb/ft^3$
ρ_g	Density of gas	$kg/m^3, lb/ft^3$
ρ_O	Density of Oil	$kg/m^3, lb/ft^3$
ρ_W	Density of Water	$kg/m^3, lb/ft^3$
μ_c	Viscosity of Continuous Phase	$Pa.sec, mPa.sec$
μ_O	Viscosity of Oil	$Pa.sec, mPa.sec$
μ_W	Viscosity of Water	$Pa.sec, mPa.sec$
α	Water Cut	$-$
β	Oil Cut	$-$
$\emptyset_{oo}$	Fraction of Inflowing Oil Entering the Bulk Oil Phase	$-$
$\emptyset_{ow}$	Fraction of Inflowing Oil Entering the Bulk Water Phase	$-$
$\emptyset_{ww}$	Fraction of Inflowing Water Entering the Bulk Water Phase	$-$
$\emptyset_{wo}$	Fraction of Inflowing Water Entering the Bulk Oil Phase	$-$
θ	Angle	$Radian$
θ^*	Delay in response signal	$second$
τ_D	Derivative time constant	$second$
τ_I	Integrating time	$second$
τ_c	Tuning time constant	$second$
γ	Interfacial tension	N/m

Abbreviations

Acronyms	Description
PC	Pressure Controller
LC	Liquid Level Controller
W	Rough Water Phase
WC	Pure or Continuous Water Phase
i	Interface
iW	Water in Interface
O	Initial or Impure or Rough Oil Phase
OC	Pure or Continuous Oil Phase
iO	Oil in interface
L	Liquid Phase

Chapter 1

1 Introduction

In order to achieve operational specifications during well production, such as saleable pipeline specification for oil and gas streams and wastewater disposal, the oil stream is expected to contain less than 1% volume of water, the gas stream is required to contain less than 5 pound-mass (lbm) water per a million standard cubic feet (MMscf), and the wastewater stream, is expected to have less than 20 parts per million (ppm) oil for overboard discharge in the Gulf of Mexico (Devold, 2010). These objectives, therefore, emphasize the need for adequate process separation system, for which gravity separation is one of the principal units utilized, during the primary stages of separation. In general gravity separation is advantageous for simplicity to utilize densities of the composite fluids in well stream to achieve separation.

Adequate separation with gravity separator usually requires that more than one gravity separator is operated in series, and these units can be installed in various configurations, in accordance with the classification of gravity separators: Two-phase or three-phase, vertical, spherical or horizontal gravity separators, and other categories. Despite this, many gravity separators still underperform, and this may be due to selection of wrong class of configuration, or in cases where the appropriate class of configuration has been selected, the sizing methodology may have been inadequate. There are various sizing methods for gravity separators, ranging from the simple "back-of-the-envelope" to other more complicated methodologies and there are several challenges associated with these methods, which include: droplet size distributions, quantification of steady state feed flows, quantification of interface between the liquid phases, velocity profiles, component performance quantification, etc. (Bothamley & Campbell/Petroskills, 2013). The quantification of liquid Interface or emulsion formation is very important, because most often well streams undergo physiochemical interaction on a molecular scale and a such poses challenges to the objectives of separation.

Crude oil emulsion is formed when liquid (water or oil) droplets of a dispersed phase are dispersed in another liquid (oil or water), the continuous phase, in case when there is sufficient mixing, presence of emulsifying agents, and at suitable temperature and pressure. This interfacial interaction can result to two major classes of emulsion systems: oil-in-water (O/W), and water-in-oil (W/O). However, the type of emulsion present determines how the emulsion system is formed and its stability (Tadros, 2013).

The formation of emulsion prevents liquid droplets of the dispersed phase from coalescing and re-forming a separate phase, which makes separation difficult, and as such, various ways have been tried, to prevent this phenomenon. There are various methods utilized to overcome the challenge posed by emulsion formation, these methods can be broadly categorized into periodic flushing and demulsification of the emulsion layer. Periodic flushing is a common method utilized when the emulsion layer is growing at a rather fast pace beyond economic control via a demulsifier. Periodic flushing is cheap but result to more difficult treatment for the resultant oil stream. However, when demulsification can be utilized within specified economic constraints, it yields better results in

separation oil and water, and thus a purer oil stream that requires less treatment, is produced. This work focuses on control of emulsion layer via demulsification, specifically via the use of chemical demulsifier.

1.1 Aims and Objectives

The aim of this work involves modelling demulsification process and control of emulsion layer (via a demulsifier) of a previously designed three-phase horizontal gravity separator, where a model for emulsion formation has been developed earlier. The objectives of this work will therefore include:

1. Investigation of a thermodynamic equation to model demulsification of the emulsion layer

2. Investigation of physical parameters that influences demulsification

3. Evaluation of practical value ranges applicable for the influencing physical parameters under investigation

4. Control of emulsion formation via the investigated equation for demulsification and influencing physical parameters

5. Simulation of the modelled horizontal gravity separator.

Chapter 2

2 Description of Gravity Separator

This section presents a summary to explore the background on horizontal gravity separator as explicitly described in previous work (Emebu, et al., 2017) based on the model developed by (Backi & Skogestad, 2017a). The model has a broad field of applications and has been applied in e.g. controller design and separation investigation (Backi, et al., 2018) as well as virtual inflow monitoring (Backi & Skogestad, 2017b), (Backi & Skogestad, 2018).

Gravity separators as stated earlier can be designed in various geometric configurations. However, gravity separators most often take two popular geometric configurations, the vertical or horizontal configuration. The geometry adopted sometimes is not based on simple logic and as such, both configurations are usually evaluated to decide which is more economical, based on desired results obtained at the lowest life-cycle cost. This work, however, focuses on horizontal gravity separator.

Horizontal gravity separators are commonly utilized in conditions, where there is large volumetric flow of gas and or liquid stream, high gas to oil ratio in the inflowing stream, foaming of fluid streams and three-phase separation processes. However, due to its high volumetric inflows, horizontal separators are quite large and as such occupy large space (but in sizing, they are smaller compared to vertical gravity separator). Furthermore, due to its geometry (i.e. decreasing horizontal volumetric flow component or large horizontal distance), its drainage ability is poor and hence difficult to clean solid particles such as sand, mud and wax pumped in or produced during the production of crude oil, and also its liquid-level control is more critical. However, it is advantageous for its ability to utilize smaller diameter for similar gas capacity as compared to a vertical separator, large liquid surface area for foam dispersion and hence a reduction of turbulence (Mokhatab, et al., 2015).

Horizontal gravity separator and its various components are listed and briefly described in Figure (2.1). (Bothamley & Campbell/Petroskills, 2013):

1. Feed pipe
2. Inlet device
3. Active separation zone: gas separation, and liquid separation section
4. Mist extractor
5. Pressure and liquid-level controller

Chapter 2

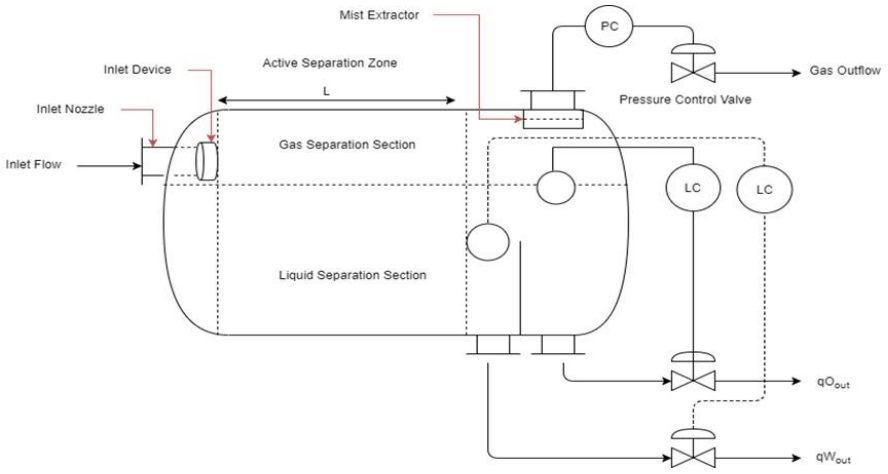

Figure 2. 1. Simplified description of horizontal gravity separator

2.1 Theory of Horizontal Gravity

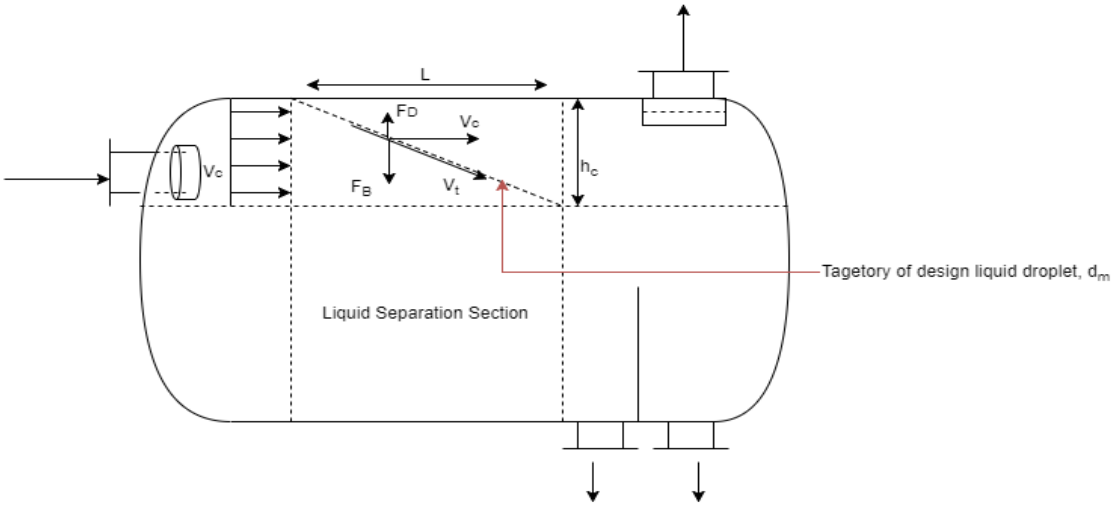

Figure 2. 2. Geometrical description of settling fluid droplet

2.1.1 Deduction of Terminal Velocity

In the active separation zone, the liquid droplets will settle at a velocity deduced from the force balance of buoyancy force, F_B and drag force, F_D (caused by relative motion of the gas phase as illustrated in Figure (2.2) and (2.3)) on the liquid droplet. When the drag force equals the buoyancy force, the droplets acceleration becomes zero and the velocity of the droplet is constant.

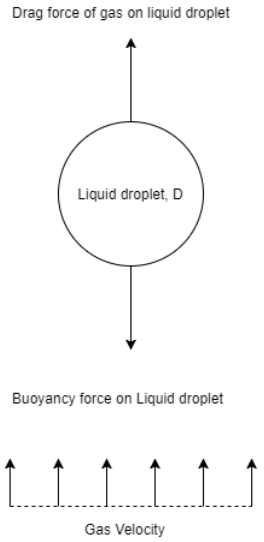

Figure 2. 3. Forces on liquid droplet in gas stream

The buoyancy, drag force and constant droplet velocity (or settling velocity) are deduced as follow:

$$F_B = m_d g - m_c g$$

where:

m_d, Mass of liquid droplets

m_c, Mass of gas displaced

g, Acceleration due to gravity, 9.81 m/s^2

Based on Archimedes principle the mass of gas or continuous phase, m_c, displaced can be deduced from the volume of the liquid droplet or dispersed phase, V_d, since the volume of gas displaced is equivalent to the volume of the liquid droplet.

$$F_B = V_d \rho_d g - V_d \rho_c g = \frac{\pi}{6} D^3 \rho_d g \; - \frac{\pi}{6} D^3 \rho_c g = \frac{\pi}{6} D^3 (\rho_d - \rho_c) g$$

$$F_D = P A_d$$

Where

P, Hydrostatic pressure

A_d, Surface area of liquid droplet

$$F_D = PA_d = (\rho_c hg)\left(\frac{\pi D^2}{4}\right) = \left(\rho_c \frac{C_D v^2}{2g} g\right)\left(\frac{\pi D^2}{4}\right) = \frac{\pi D^2}{8}\rho_c C_D v^2$$

At equilibrium:

$$F_B = F_D$$

$$\therefore \frac{\pi}{6} D^3(\rho_d - \rho_c)g = \frac{\pi D^2}{8}\rho_c C_D v^2$$

$$v \cong v_t = \sqrt{\frac{4gD(\rho_d - \rho_c)}{3\rho_c C_D}} \quad (2.1)$$

Where:

D, Liquid droplet diameter, m

ρ_d, Dispersed or liquid phase density, kg/m^3

ρ_c, Continuous or gas phase density, kg/m^3

C_D, Drag coefficient of particle, dimensionless

v_t, Terminal gas velocity necessary for liquid droplet to settle out of gas, m/s

Equation (2.1) is the principal equation of gravity separation. However, the evaluation of terminal velocity, v_t is not readily implementable because drag coefficient, C_D is also a function of v_t. Hence, both parameters are dependent on each other. However, there are two fundamental ways to get around this, namely correlation of experimental parameters into Equation (2.1), and simplified, empirical models and analytical correlation of C_D. However, the analytical correlation of C_D is applicable and as such discussed in the proceeding section.

2.1.1.1 Analytical correlation of C_D

The drag coefficient, C_D has been deduced to be a function of the shape of the droplet and the Reynolds number, Re of the flowing gas, and since it can be reasonably inferred that the liquid droplet, D is approximately spherical. Then the Reynolds number is as defined in Equation (2.2).

$$Re = \frac{Dv_t\rho_c}{\mu_c} \tag{2.2}$$

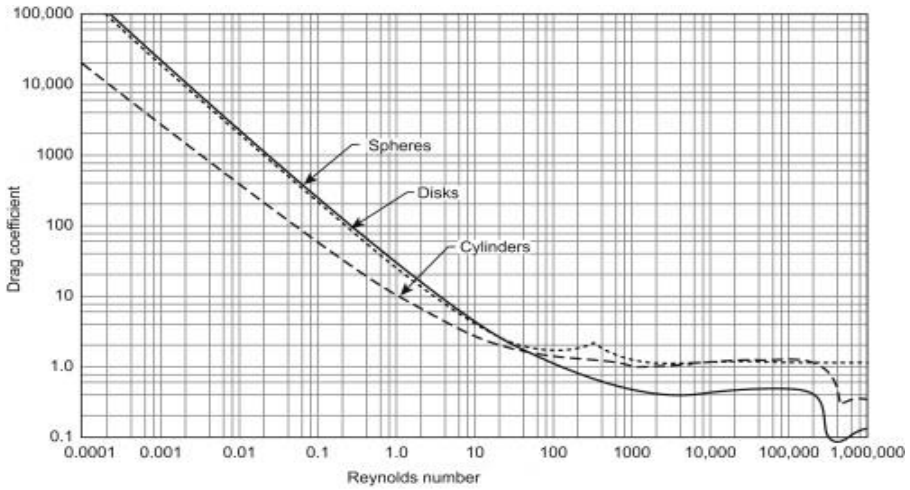

Figure 2. 4. Relationship between drag coefficient and Reynolds number (Moshfeghian, 2015)

Figure (2.4) shows the relationship between drag coefficient and droplet Reynolds number for liquid droplet. In this form, trial and error solution is required since liquid droplet size and terminal velocity are unknown.

In order to avoid this, the drag coefficient is presented as a function of the product of drag coefficient and Reynolds number squared, so that the terminal velocity term is eliminated from the expression. This is shown in Figure (2.5).

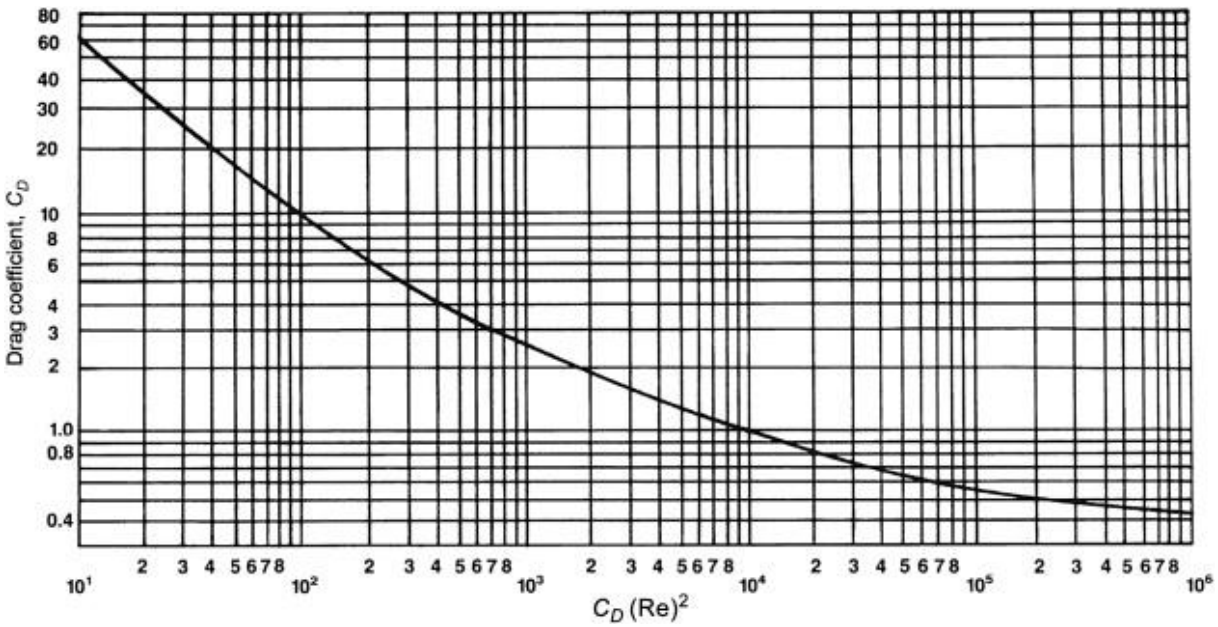

Figure 2. 5.Drag coefficient for spherical liquid droplet (Moshfeghian, 2015)

The expression for, $C_D Re^2$ as shown in Figure (2.5) in the estimation of drag is as given in Equation (2.3).

$$C_D Re^2 = \frac{4g\rho_c(\rho_d - \rho_c)D^3}{3\mu_c^2} \tag{2.3}$$

Observation of Equation (2.3) shows that the drag coefficient will be very small at high Reynolds numbers. Estimated $C_D Re^2$ (or modified form of $C_D Re^2$) can be used to deduce C_D from Figure (2.5).

In computing C_D via Equation (2.3) and Figure (2.5), there are limitations in trying to estimate the terminal velocity. These limitations include (Mohammed, 2013): wall effects, which decrease the terminal velocity in practice, effects of other droplets are neglected, the approach is for spherical droplets, which is not the case for all droplets, the value of liquid droplet is not readily available and still needs to be estimated and liquid droplets can coalesce with other droplets, changing the size of the diameter.

In order to have a more accurate estimation of liquid droplet diameter, an alternative to using Equation (2.3) and Figure (2.5), the curve shown in Figure (2.4) can be simplified into three sections based on the present flow regime in the separator, shown in Figure (2.6). An approximate relationship between drag coefficient and Reynolds number can then be deduced. These expressions can be substituted into Equation (2.1), to yield Stokes', Intermediate and Newton's settling laws. This computation is made possible via a reliable estimate of liquid droplet diameter given in Equation (2.4) (Bahadori, 2014).

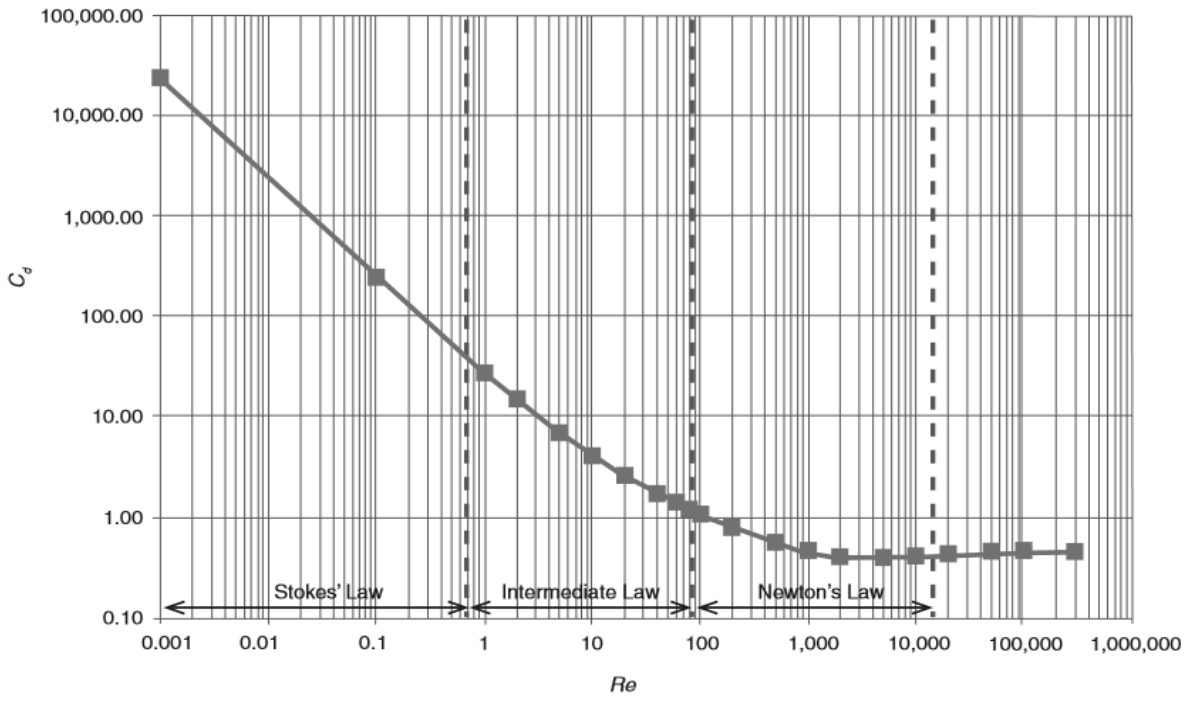

Figure 2. 6. Sections based on flow regime of relation between drag coefficient and Reynolds number (Mark Bothamley, 2013)

$$D = k\left(\frac{\mu_c^2}{g\rho_c(\rho_d - \rho_c)}\right)^{0.33} \tag{2.4}$$

Where, k is a proportionality constant, based on the flow regime found from Figure (2.4) or (2.6) with μ_c, being the viscosity of the continuous phase in $mPa\ sec$ and other parameters are in SI unit.

2.1.1.1.1 Stokes' settling law

In regimes of low Reynolds numbers ($Re \leq 2$), corresponding to laminar flow, a linear relationship exists between the drag coefficient and the Reynolds number, such that, $C_D \cong 24\ Re \cong 24\mu_c/Dv_t\rho_c$, and when substituted into Equation (2.1) yield the terminal velocity given in Equation (2.5), known as Stokes' settling law, with all parameters in SI units (Tanaka & Iinoya, 1970).

$$v_t = \frac{gD^2(\rho_d - \rho_c)}{18\mu_c} \tag{2.5}$$

The liquid droplet diameter corresponding to $Re \cong 2$ can be found using a value of 0.033 as proportionality constant, k in Equation (2.4).

Stokes' settling law is typically applicable for small liquid droplet sizes and/or liquid phases with relatively high viscosity (Bahadori, 2014). This is the model for terminal velocity used in this work.

2.1.1.1.2 Intermediate Settling law

In intermediate flow regime with $2 \leq Re \leq 500$, the drag coefficient is found to be, $C_D \cong 18.5/Re^{0.6}$ (Mostika, et al., 1999), and when substituted into Equation (2.1) gives the terminal velocity in Equation (2.6), known as the intermediate settling law (Gas Processors Suppliers Association, 2014).

$$v_t = \frac{0.29g^{0.714}D^{1.142}((\rho_d - \rho_c)^{0.714}}{\rho_c^{0.286}\mu_c^{0.428}} \tag{2.6}$$

Where all parameters are in SI unit, and the liquid droplet diameter corresponding to $Re \cong 500$ can be found using a value of 0.435 as proportionality constant, k in Equation (2.4) (Mark Bothamley, 2013).

2.1.1.1.3 Newton's law

For flow regime with $500 \leq Re \leq 200000$, the drag coefficient is, $C_D \cong 0.44$. Substituting C_D into Equation (2.1) gives the Newton's settling law as shown in Equation (2.7). This is usually applicable for separation of large droplets or droplets from a gas phase.

$$v_t = 1.74\sqrt{\frac{gD(\rho_d - \rho_c)}{\rho_c}} \tag{2.7}$$

Where all parameters are in SI units. The liquid droplet diameter corresponding to $Re \cong 200000$ can be found using a value of 23.64 as proportionality constant, k in Equation (2.7) (Bahadori, 2014).

Chapter 3

3 Crude Oil Emulsion Formation

Interface or Emulsion is a dispersed system made of two interacting immiscible liquids, in which liquid droplets of one phase are dispersed in another liquid continuous phase. There are different forms of crude oil emulsions, which are mainly: oil-in-water (O/W) and water-in-oil (W/O)(Tadros, 2013). The formation of crude oil emulsion is initiated by turbulence caused during well production processes and subsequently stabilized by emulsifiers present in the production streams. The form of emulsion created is usually dependent on the emulsifier present (Nour, et al., 2008).

The extent of turbulence and amount of emulsifier are critical during emulsion formation. The sources of turbulence during well production include: bottom hole pumps, flow lines, production headers, valves, fittings, and chokes, etc. Emulsifiers present are e.g. surface-active agents found naturally in crude oil, such as asphaltenes, resins, organic acids and bases as well as other surfactants present, which can be found in e.g. drilling fluids, corrosion inhibitors, scale inhibitors, etc. Emulsifiers are also present in the form of finely divided solids, found during oil production, such as clay and shale particles, sand and silt, corrosion products, and drilling muds, etc. (Simanzhenkov & Idem, 2003).

3.1 Mechanism of Crude-Oil Emulsion Formation

Organic and inorganic solids consist mainly of clay minerals, asphaltenes, resins, and wax. These solids stabilize emulsions by adsorbing the polar constituents of crude oil, resulting in modification of its wettability, and thus allowing them to be attached on the water-oil interface. In general, the degree to which solids increase emulsion stability depends on several factors such as particle size, shape and morphology, density, concentration and surface coverage as well as wettability (Elsharkawy, et al., 2008).

Asphaltenes and resins are mainly polar hetero-compounds that contribute significantly to crude oil emulsion stabilization. Asphaltenes can also precipitate from crude oil under unfavourable conditions of temperature and pressure, and as such can result in flow restriction around the wellbore, thus inducing turbulence. The occurrence of turbulence initiates emulsion formation. Furthermore, asphaltenes enhance stabilization of the initiated emulsion on the produced crude oil fed to surface units, such as gravity separator, by accumulating on liquid interface. The accumulation of asphaltenes on liquid interface leads to the formation of rag layer, that reduces the fluid capacity and thus the residence time of separation (Elsharkawy, et al., 2008).

Chapter 3

3.2 Model for Emulsion Formation

The model for emulsion formation as explicitly described in previous work (Backi & Skogestad, 2017a), (Backi, et al., 2018) and is summarized in the proceeding section.

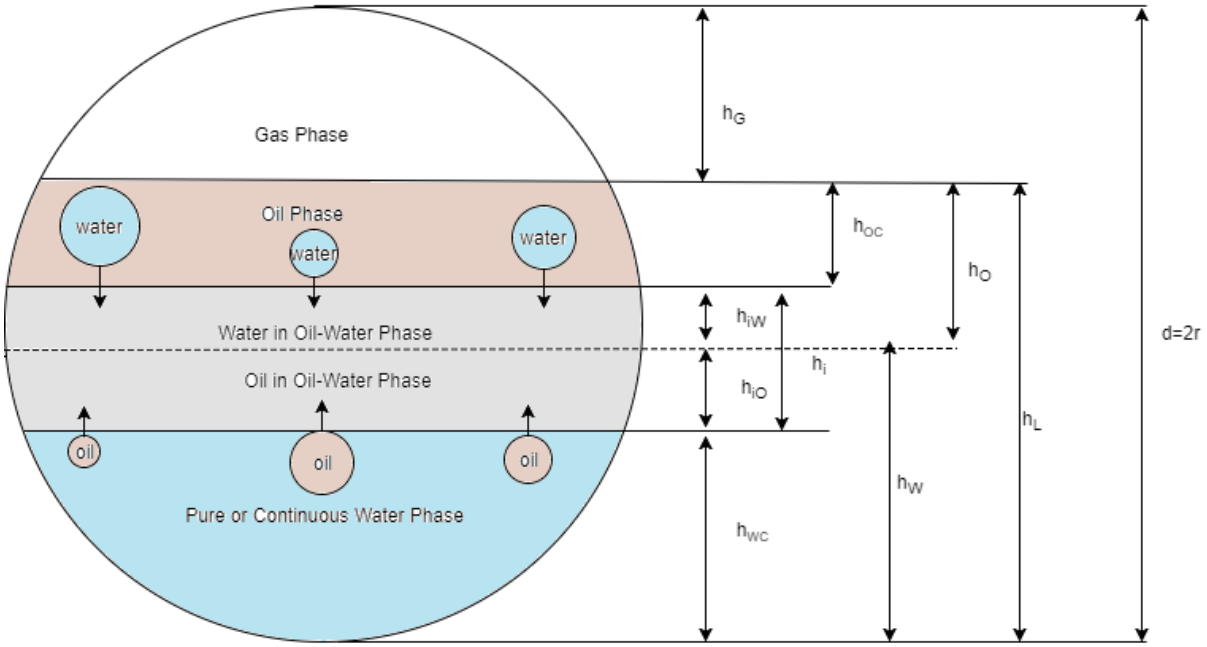

Figure 3. 1. Cross- sectional area of phases in horizontal gravity separators

The liquid emulsion or interface is composed of a mixture of water and oil. The water component, iW is composed of water initially dispersed in the oil-continuous phase,OC that settles under the influence of gravity and difference in density to a layer beneath the oil-continuous phase. Accordingly, the oil component, iO consists of oil initially dispersed in the water-continuous phase, WC that rise under the influence of buoyancy and density difference to a layer above the water-continuous phase. Hence, the two layers iW and iO form the interface, i as illustrated in Figure (3.2).

In modelling the interface, for simplicity it is assumed that:

1. The oil-interface, iO plus the water-continuous phase,WC define the water phase i.e. $W = WC + iO$ as illustrated in Figure (3.1) and Figure (3.2).

2. Accordingly, the water-interface, iW plus the oil-continuous phase, OC defines the oil phase i.e. $O = OC + iW$ as illustrated in Figure (3.1) and (3.3).

3.2.1 Oil in Oil-water Interface, iO

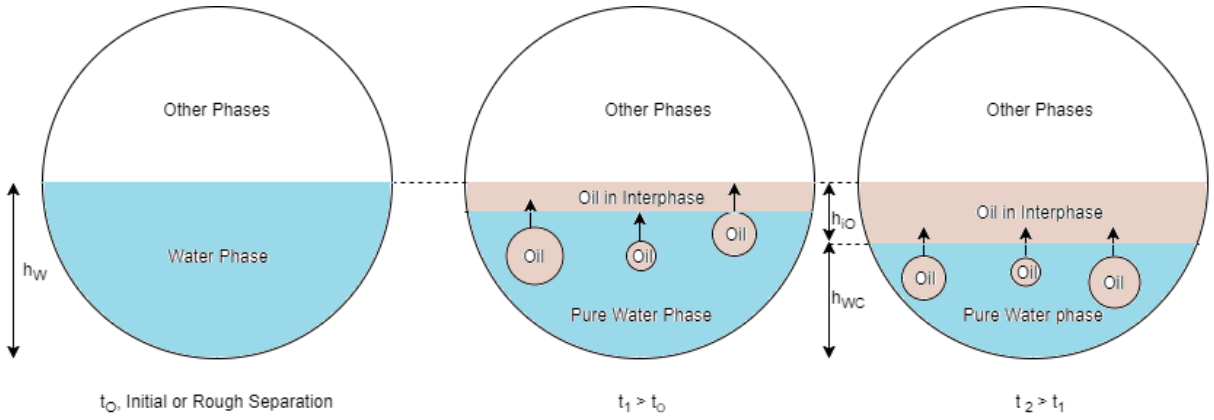

Figure 3. 2. Cross-sectional area of gravity separator showing growth of oil in interface with time

Assuming constant oil density in the oil-water interface, the volumetric rate of change in the oil-water interface can be expressed as:

$$\frac{dV_{iO}}{dt} = \frac{V_{OoW}}{V_O} q_{L,in}(\beta \emptyset_{OW}) - q_{iO,out} \tag{3.1}$$

The change in area of the oil-water interface section with respect to the length of the active separation zone is given as, $dA_{iO}/dt = (dV_{iO}/dt)\,(1/L)$, where A_{io} is the area of a circular segment with its height, h_{iO} and is deduced as:

$$A_{iO} = A_W - A_{WC} = A_W - A_{W-iO}$$

i.e. explicitly expressed as $A_{iO} = A_W - (A_W - A_{iO})$, however for appropriate derivation of A_{iO} the expression $A_{iO} = A_W - A_{W-iO}$ is used as shown in Figure (3.1) and (3.2).

where,

$$A_{W-iO} = \frac{r^2}{2}\left[2cos^{-1}\left(\frac{r - h_{W-iO}}{r}\right) - \sin\left(2cos^{-1}\left(\frac{r - h_{W-iO}}{r}\right)\right)\right] \tag{3.2}$$

The approach for derivation of dh_{io}/dt is presented in the proceeding steps:

$$\frac{dA_{iO}}{dt} = \frac{dA_W}{dt} - \frac{dA_{W-iO}}{dt} \tag{3.3}$$

The derivation of dA_{W-io}/dt is also same procedure as earlier deduced for dA_W/dt, which is given as,

$$\frac{dA_{W-iO}}{dt} = 2\sqrt{(h_W - h_{iO})(2r - (h_W - h_{iO}))}\frac{dh_{W-iO}}{dt}$$

where,

$h_{W-iO} = h_W - h_{iO}$

$dh_{W-iO}/dt = dh_W/dt - dh_{iO}/dt$

Hence,

$$\frac{dA_{W-iO}}{dt} = 2\sqrt{(h_W - h_{iO})(2r - (h_W - h_{iO}))}\left(\frac{dh_W}{dt} - \frac{dh_{iO}}{dt}\right) \tag{3.4}$$

Substituting the Equation (3.4) into Equation (3.3) yields Equation (3.5)

$$\frac{dA_{iO}}{dt} = 2\sqrt{h_W(2r - h_W)}\frac{dh_W}{dt} - 2\sqrt{(h_W - h_{iO})(2r - (h_W - h_{iO}))}\left(\frac{dh_W}{dt} - \frac{dh_{iO}}{dt}\right)$$

$$\frac{dA_{iO}}{dt} = 2\sqrt{(h_W - h_{iO})(2r - (h_W - h_{iO}))}\frac{dh_{iO}}{dt} + 2\left(\sqrt{h_W(2r - h_W)} - \sqrt{(h_W - h_{iO})(2r - (h_W - h_{iO}))}\right)\frac{dh_W}{dt}$$

$$\frac{dh_{iO}}{dt} = \frac{\frac{dA_{iO}}{dt} - 2\left(\sqrt{h_W(2r - h_W)} - \sqrt{(h_W - h_{iO})(2r - (h_W - h_{iO}))}\right)\frac{dh_W}{dt}}{2\sqrt{(h_W - h_{iO})(2r - (h_W - h_{iO}))}}$$

$$\frac{dh_{iO}}{dt} = \frac{\frac{1}{L}\frac{dV_{iO}}{dt} - 2\left(\sqrt{h_W(2r - h_W)} - \sqrt{(h_W - h_{iO})(2r - (h_W - h_{iO}))}\right)\frac{dh_W}{dt}}{2\sqrt{(h_W - h_{iO})(2r - (h_W - h_{iO}))}}$$

$$\frac{dh_{iO}}{dt} = \frac{1}{2L\sqrt{(h_W - h_{iO})(2r - (h_W - h_{iO}))}}\frac{dV_{iO}}{dt} - \left(\frac{\sqrt{h_W(2r - h_W)} - \sqrt{(h_W - h_{iO})\big(2r - (h_W - h_{iO})\big)}}{\sqrt{(h_W - h_{iO})\big(2r - (h_W - h_{iO})\big)}}\right)\frac{dh_W}{dt}$$

$$\frac{dh_{iO}}{dt} = \frac{1}{2L\sqrt{(h_W - h_{iO})(2r - (h_W - h_{iO}))}}\frac{dV_{iO}}{dt} - \left(\frac{\sqrt{h_W(2r - h_W)}}{\sqrt{(h_W - h_{iO})\big(2r - (h_W - h_{iO})\big)}} - 1\right)\frac{dh_W}{dt}$$

Substituting for dh_W/dt, leads to,

$$\frac{dh_{iO}}{dt} = \frac{1}{2L\sqrt{(h_W - h_{iO})(2r - (h_W - h_{iO}))}}\frac{dV_{iO}}{dt} - \left(\frac{\sqrt{h_W(2r - h_W)}}{\sqrt{(h_W - h_{iO})\big(2r - (h_W - h_{iO})\big)}} - 1\right)\frac{1}{L}\frac{dV_W}{dt}\frac{1}{2\sqrt{h_W(2r - h_W)}}$$

$$\frac{dh_{iO}}{dt} = \frac{1}{2L\sqrt{(h_W - h_{iO})(2r - (h_W - h_{iO}))}}\frac{dV_{iO}}{dt} - \frac{1}{2L}\left(\frac{1}{\sqrt{(h_W - h_{iO})\big(2r - (h_W - h_{iO})\big)}} - \frac{1}{\sqrt{h_W(2r - h_W)}}\right)\frac{dV_W}{dt} \quad (3.5)$$

3.2.2 Water in Oil-water Interface, iW

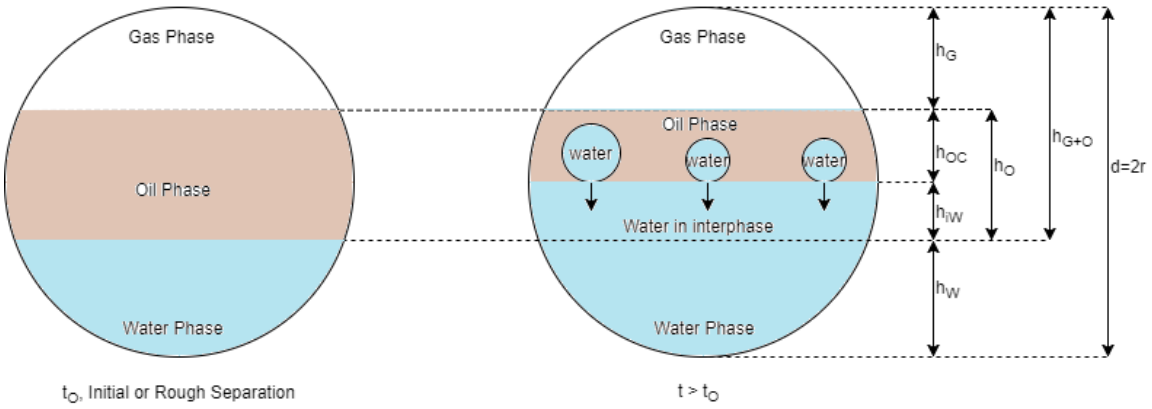

Figure 3. 3. Cross-sectional area of gravity separator showing growth of water in interface with time

Assuming constant water density in the oil-water interface, the rate of changes volume oil in oil-water interface can be expressed as:

$$\frac{dV_{iW}}{dt} = \frac{V_{WoO}}{V_W} q_{L,in}(\alpha \emptyset_{WO}) - q_{iW,out} \tag{3.6}$$

The change in area of the oil-water interface section with respect to the length of the active separation zone is given as, $dA_{iW}/dt = (dV_{iW}/dt)\,(1/L)$, where A_{iW} is the area of a circular segment is deduced as earlier assumed and as shown in Figure (3.1) and (3.3) with its height (sagitta), h_{iW}:

$$A_{iW} = A_{G+O+iW} - A_{G+O}$$

where,

$$A_{G+O+iW} = \frac{r^2}{2}\left[2cos^{-1}\left(\frac{r - h_{G+O+iW}}{r}\right) - \sin\left(2cos^{-1}\left(\frac{r - h_{G+O+iW}}{r}\right)\right)\right]$$

$$A_{G+O} = \frac{r^2}{2}\left[2cos^{-1}\left(\frac{r - h_{G+O}}{r}\right) - \sin\left(2cos^{-1}\left(\frac{r - h_{G+O}}{r}\right)\right)\right]$$

The approach for derivation of dh_{iW}/dt is presented in the proceeding steps:

$$\frac{dA_{iW}}{dt} = \frac{dA_{G+O+iW}}{dt} - \frac{dA_{G+O}}{dt}$$

Following same procedures as derived for dA_L/dt earlier, dA_{G+O+iW}/dt and dA_{G+O}/dt are deduced.

$$\frac{dA_{G+O+iW}}{dt} = 2\sqrt{h_{G+O+iW}(2r - h_{G+O+iW})}\frac{dh_{G+O+iW}}{dt}$$

But, $h_{G+O+iW} = 2r - h_W$ as shown in Figure (3.1) and (3.3)

$$\frac{dA_{G+O+iW}}{dt} = 2\sqrt{(2r - h_W)(h_W)}\frac{dh_{G+O+iW}}{dt}$$

Therefore, $dh_{G+O+iW}/dt = d(2r - h_W)/dt = -\ dh_W/dt$

$$\frac{dA_{G+O+iW}}{dt} = -2\sqrt{(2r - h_W)h_W}\frac{dh_W}{dt}$$

similarly,

$$\frac{dA_{G+O}}{dt} = 2\sqrt{h_{G+O}(2r - h_{G+O})}\frac{dh_{G+O}}{dt}$$

where, $h_{G+O} = 2r - h_W - h_{iW}$ as shown in Figure (3.1) and (3.3)

$$\frac{dA_{G+O}}{dt} = 2\sqrt{(2r - h_W - h_{iW})(h_W + h_{iW})}\frac{dh_{G+O}}{dt}$$

Therefore $dh_{G+O}/dt = d(2r - h_W - h_{iW})/dt = -\ (dh_W/dt + dh_{iW}/dt)$

$$\frac{dA_{G+O}}{dt} = -2\sqrt{(2r - h_W - h_{iW})(h_W + h_{iW})}\left(\frac{dh_W}{dt} + \frac{dh_{iW}}{dt}\right)$$

$$\therefore \frac{dA_{iW}}{dt} = -2\sqrt{(2r-h_W)(h_W)}\left(\frac{dh_W}{dt}\right) - \left(-2\sqrt{(2r-h_W-h_{iW})(h_W+h_{iW})}\left(\frac{dh_W}{dt}+\frac{dh_{iW}}{dt}\right)\right)$$

$$\frac{dA_{iW}}{dt} = -2\sqrt{(2r-h_W)(h_W)}\left(\frac{dh_W}{dt}\right) + 2\sqrt{(2r-h_W-h_{iW})(h_W+h_{iW})}\left(\frac{dh_W}{dt}+\frac{dh_{iW}}{dt}\right)$$

$$\frac{dA_{iW}}{dt} = 2\sqrt{(2r-h_W-h_{iW})(h_W+h_{iW})}\left(\frac{dh_W}{dt}+\frac{dh_{iW}}{dt}\right) - 2\sqrt{(2r-h_W)(h_W)}\left(\frac{dh_W}{dt}\right)$$

$$\frac{dh_{iW}}{dt} = \frac{\frac{dA_{iW}}{dt} + 2\left(\sqrt{(2r-h_W)(h_W)} - \sqrt{(2r-h_W-h_{iW})(h_W+h_{iW})}\right)\left(\frac{dh_W}{dt}\right)}{2\sqrt{(2r-h_W-h_{iW})(h_W+h_{iW})}}$$

$$\frac{dh_{iW}}{dt} = \frac{\frac{1}{L}\frac{dV_{iW}}{dt} + 2\left(\sqrt{(2r-h_W)(h_W)} - \sqrt{(2r-h_W-h_{iW})(h_W+h_{iW})}\right)\left(\frac{dh_W}{dt}\right)}{2\sqrt{(2r-h_W-h_{iW})(h_W+h_{iW})}}$$

$$\frac{dh_{iW}}{dt} = \frac{1}{2L\sqrt{(2r-h_W-h_{iW})(h_W+h_{iW})}}\frac{dV_{iW}}{dt} + \left(\sqrt{\frac{(2r-h_W)(h_W)}{(2r-h_W-h_{iW})(h_W+h_{iW})}} - 1\right)\frac{dh_W}{dt}$$

$$\frac{dh_{iW}}{dt} = \frac{1}{2L\sqrt{(2r-h_W-h_{iW})(h_W+h_{iW})}}\frac{dV_{iW}}{dt} + \left(\sqrt{\frac{(2r-h_W)(h_W)}{(2r-h_W-h_{iW})(h_W+h_{iW})}} - 1\right)\frac{1}{2L\sqrt{h_W(2r-h_W)}}\frac{dV_W}{dt}$$

$$\frac{dh_{iW}}{dt} = \frac{1}{2L\sqrt{(2r-h_W-h_{iW})(h_W+h_{iW})}}\frac{dV_{iW}}{dt} + \frac{1}{2L}\left(\frac{1}{\sqrt{(2r-h_W-h_{iW})(h_W+h_{iW})}} - \frac{1}{\sqrt{h_W(2r-h_W)}}\right)\frac{dV_W}{dt}$$

$$\frac{dh_{iW}}{dt} = \frac{1}{2L\sqrt{(2r-h_W-h_{iW})(h_W+h_{iW})}}\frac{dV_{iW}}{dt} - \frac{1}{2L}\left(\frac{1}{\sqrt{h_W(2r-h_W)}} - \frac{1}{\sqrt{(2r-h_W-h_{iW})(h_W+h_{iW})}}\right)\frac{dV_W}{dt} \quad (3.7)$$

The expression for the volumetric rate of change for water, dV_w/dt is as given in Equation (3.8).

$$dV_w/dt = q_{W,in} - q_{W,out} = q_{L,in}(\alpha \emptyset_{WW}) + q_{iW,out} - q_{W,out} \tag{3.8}$$

Chapter 4

4 Demulsification of Emulsion

The formation of emulsion poses problems during well production and transportation of produced fluids to processing plants. This is a costly problem, both in terms of chemicals used and losses in the production process. Therefore, emulsion formation is a problem, that must be tackled at all times. It can be solved by breaking up the emulsion, this process is called demulsification. There are different methods of demulsification, a single or a combination of these methods can be utilized:

1. Thermal demulsification
2. Electrical demulsification (electrostatic coalescence)
3. Mechanical demulsification
4. Chemical demulsification (chemical treatment, demulsifier)

4.1.1 Thermal demulsification

Thermal demulsification method applies the principle of temperature alteration to demulsify the emulsion and thus enhances separation. Thermal demulsification enhances separation in two ways. First, by decreasing the viscosity of the emulsion, thereby allowing water droplet to drain through the emulsion. Secondly, as temperature tends towards the phase-inversion temperature of the emulsion, the emulsion destabilizes (Kelland, 2014). Based on this method, the outflow of separated oil and water phases, $q_{i,out}$ is a function of temperature, T of the separation zone, i.e. $q_{i,out} = f(T)$. There are different heating devices utilized in this method, which can be generally classified into direct or indirect heating devices.

4.1.2 Electrical demulsification (Electrostatic coalescence)

Electrostatic coalescence is used industrially to demulsify emulsion via application of electric field to liquid phases in the gravity separation zone. Electrostatic coalescence is considered an ideal demulsification method because it applies physical principles, which makes recycling of the phases feasible. Application of a high electric field can be established across the emulsion, since the oil phase is non-conductive, but the water phase is conductive. This leads to the following phenomena (Larson, et al., 1994), (Stewart & Arnold, 2007):

1. Droplets become attracted to the electrode due to induced charges. When alternating current is applied, vibration of liquid droplets is initiated, however smaller droplets vibrate more vigorously compared to larger ones thus promoting coalescence. However, when direct current is applied, droplets tend to be accumulated on the electrodes, forming larger droplets that can be separated.

2. Droplets become polarized, causing the positive and negative poles of the droplets to attract, thus leading to coalescences.

3. The created electric field weakens the film of the emulsifier around the liquid droplets. This weakened film becomes easily broken when droplets collide, thus prompting coalescence.

4.1.3 Mechanical demulsification

Mechanical methods of demulsification include the use of physical mechanism such as vibration and centrifugation to enhance separation of emulsified liquid phases. These methods, however, don't seem applicable in gravity separator devices.

4.1.4 Chemical demulsification (chemical treatment, demulsifier)

The application of demulsifying agents to the emulsion is the most common method of demulsification, and hence the method of focus for this work. Demulsification is characterized by proper chemical selection for a given emulsion, quantification of the chemical, optimal mixing of the chemical with the emulsion and the retention time in the separator. Chemical demulsifiers include combinations of the following chemicals: Esters, di-epoxides, resins, polyalkylene, glycols, sulfonates, polyester amines, oxyalkylated phenols, oxyalkylated polyamines, alkanol amines etc. These demulsifiers are generally classified into the four types anionic, cationic, non-ionic, and amphoteric (Al-Sabagh, et al., 2011).

4.2 Mixing of demulsifier

Mixing of the demulsifier with the emulsion is necessary for adsorption of the demulsifier on the oil-water interface however optimal agitation is required to prevent re-emulsification. In practice, the demulsifier is added continuously (at a rate determined by the field trials), to ensure steady mixing of the demulsifier and the emulsion. Batch addition of demulsifiers is avoided in practice (SPE International, 2015).

4.3 Quantification of demulsifier

The quantity of demulsifier to be added is important because a small dosage of demulsifier cannot break the emulsion while a larger dosage can cause problems (Amani, et al., 2017). Determination of the optimal dosage is quite difficult due to constraints such as types of crude oil, types of demulsifiers, separation equipment and variations in product specifications.

Chapter 4

Emulsions formed during primary or secondary oil recovery require demulsifier rates in the range of less than 10 to greater than 100 ppm, based on total production rate. Most often, in practice, it is between 10 - 60 ppm. Emulsions formed during tertiary oil recovery, especially during surfactant or micellar flooding, require demulsifier rates in the range of 100 ppm and higher in extreme cases. Generally, in practice, heavy crude oils require larger dosage than light oils, and in addition, the dosage during summer and winter time is different (Manning & Thompson, 1995) (Kokal, et al., 2002).

WVT industries recommended that total demulsifier dosages vary between 1500 and 4000 ppm to the total amount of the oil-water emulsion. It is also recommended that if higher dosages fail, the dosage should even be reduced, and that lower dosages of 3000 ppm usually improve the demulsification (WVT Industries, 2014).

The interfacial concentration of commercial demulsifiers adsorbed at the interface can be deduced by Gibb's Isotherm, given in Equation (4.1).

$$Z = \frac{-1}{RT}\frac{d\gamma}{d\ln C} \tag{4.1}$$

Where,

Z, concentration of demulsifier species adsorbed at the interface, mol/m^2

R, ideal gas constant, $8.3141\, J/Kmol$

T , temperature of the crude assay, K

$d\gamma/d\ln C$, Interfacial activity, N/m

The molecular area occupied by a demulsifier molecule adsorbed at the interface can be estimated via Equation (4.2).

$$A = \frac{1}{N_a Z} \tag{4.2}$$

Where, A, is the molecular area of the adsorbed demulsifier species, $Å^2$ and N_a, is the Avogadro's number, $6.02 \times 10^{23} mole^{-1}$.The interfacial properties of three commercial demulsifier bases is presented in Table (4.1).

Table 4. 1. Interfacial properties of some commercial demulsifier bases

Demulsifier base	Molecular structure	$Z, mol/m^2$	A, $Å^2$
D1	Linear	1.43×10^{-6}	116
D2	Star	1.18×10^{-6}	141
D3	Branched	2.96×10^{-6}	56

In practice, demulsifiers are injected as early as possible (e.g. at the wellhead or even downhole). This provides enough time for demulsifier to be adsorbed and prevents possible downstream emulsion formation. Injecting the demulsifier upstream of a pump ensures adequate mixing and minimizes emulsion formation inside the pump. Mild mixing (e.g. during pipe flow and at design velocities) can accelerate chemical dispersion and flocculation of the water droplets (Manning & Thompson, 1995).

4.4 Mechanism of chemical demulsification

Demulsification of emulsion occurs in the following sequential steps: Flocculation or coalescence. Either flocculation or coalescence can be the rate-determining step in emulsion breakage. While the final step involves the separation of the water and oil phases via creaming and sedimentation (Tadros, 2013), (Pradilla, et al., 2017), (Kokal, et al., 2002).

4.4.1 Flocculation

Flocculation is a demulsification process that involves aggregation of smaller droplets into larger droplets. This is induced by the van der Waals force of attraction, because there is insufficient repulsion to keep the liquid droplets far enough to render the van der Waals force of attraction weak (Tadros, 2013). This is hardly the case in crude oil emulsion formation and demulsification, but still contributes to emulsion breakage (Kokal, et al., 2002).

4.4.2 Coalescence

Coalescence is a demulsification step, which involves combination of water or oil droplets in an emulsion. It leads to the depletion of an emulsion by forming bigger droplets from smaller droplets and hence the number of dispersed waters and liquid droplets in the emulsion decreases (Tadros, 2013). This is usually the main demulsification mechanism in crude oil demulsification processes (Al-Sabagh, et al., 2011).

4.4.3 Creaming and Sedimentation

On aggregation of liquid droplets in the emulsion phase, external forces (such gravitational or centrifugal forces) greater than the thermal motion of the droplets (i.e. Brownian motion), begin to act on the droplets. Sedimentation involves the settling of demulsified water droplets large enough to be acted upon by gravitational force because of their large density. While creaming denotes the rising of demulsified oil droplets under the influence of buoyancy force due to their lower density (Tadros, 2013). This mechanism is illustrated in Figure (2.3) and it's assumed to obey the Stokes' settling law, Equation (2.5).

4.5 Disadvantages of demulsifier

In the process of tackling the problem of emulsification of well streams, via the use of demulsifiers. There have been some shortcomings in using some demulsifiers, and they include (Manning & Thompson, 1995) (Kang, et al., 2013):

1. Toxicity to the environment, since traces of demulsifiers may remain in disposed water streams.
2. High cost in energy required for mixing of demulsifiers. Many demulsifiers take long time to accomplish demulsification.
3. Some demulsifiers are more or only effective for certain types of crude oil emulsions.
4. The use of demulsifiers only can be costly.

4.6 Model for Demulsification

Demulsification rate of separated phases out of the emulsion layer, has been assumed to significantly depend on the mechanism of coalescence, and as such on the coalescence time, t_c, of aggregating droplets. Reports from literature suggest that the interfacial tension of the liquid droplets, γ, determines how fast the liquid droplets aggregate, via changes on the interaction energy between molecules that form the emulsion layer. This change in interaction energy is quantified by a so-called retarded Hamaker constant, Ha. Grimes, 2012 proposed a relationship on how interfacial tension, and consequently interaction energy of molecules in emulsions influence coalescence and is as given in Equation (4.3) -(4.4).

$$q_{i,out} = A_i \int_o^\infty \frac{r}{3\tau_c} f(r)dr \cong \frac{A_i r_d}{3t_c} \tag{4.3}$$

Where, $A_i = L\sqrt{8h_W r - 4h_W^2}$, is the interfacial area, r_d, is the radius of liquid droplets that form the emulsion layer, r, denotes the radius of the separator, h_W, indicates the instantaneous height of the impure water phase, and t_c, is the coalescence time given in Equation (4.4).

$$t_c = 1.046 \frac{\mu_c(\rho_d - \rho_c)g_z r_d^{9/2}}{\gamma^{3/2} Ha^{1/2}} \tag{4.4}$$

Chapter 5

5 Investigating the effect of interfacial tension, Hamaker constant and droplet size on crude oil-water emulsion outflow

5.1 Evaluation of Interfacial tension and Hamaker constant

In order to deduce appropriate values and pairing for interfacial tension, γ, and retarded Hamaker constant, Ha, for Equation (4.4), which are required in deducing the outflow of crude oil-water emulsion in Equation (4.3) as proposed by Grimes (Grimes, 2012). A vector set for γ ranging from 1×10^{-3} to $60 \times 10^{-3}\ N/m$ and corresponding Ha ranging from 1×10^{-20} to $1 \times 10^{-40}\ Jm$ were initially set. However, based on data from literature (Lyons, et al., 2004), and advice from industrial partners, γ for crude oil-water emulsion can be as high as approximately $30 \times 10^{-3} - 32 \times 10^{-3}\ N/m$, while the minimum γ attainable for demulsified crude oil-water emulsion is approximately $5 \times 10^{-3} N/m$, however in some cases it can be lower, therefore for simplicity, the incremental changes for investigation of γ was set as $5 \times 10^{-3} N/m$. Likewise, rough estimates for incremental changes of Ha were set in the order of $1 \times 10^{-20}, 1 \times 10^{-22}, \ldots, 1 \times 10^{-38}\ and\ 1 \times 10^{-40} Jm$. These proposed initial boundaries were simulated, to deduce acceptable value band, that fit with the expectations of this case study. Results are as shown in Figure (5.1a) and (5.1b) for both $1\mu m$ minimum and $500\mu m$ maximum droplet radii for oil and water.

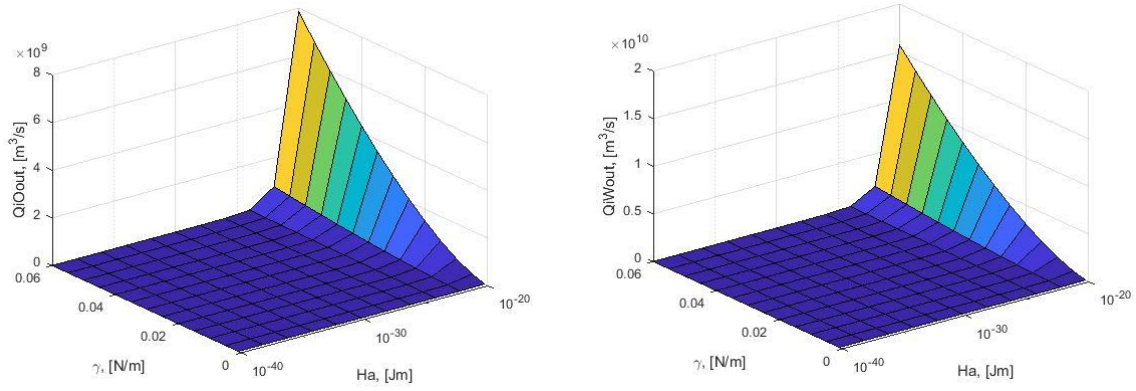

i. Oil emulsion phase ii. Water emulsion phase

Figure 5.1 a. Effect of interfacial tension and Hamaker constant on emulsion outflow for small droplets

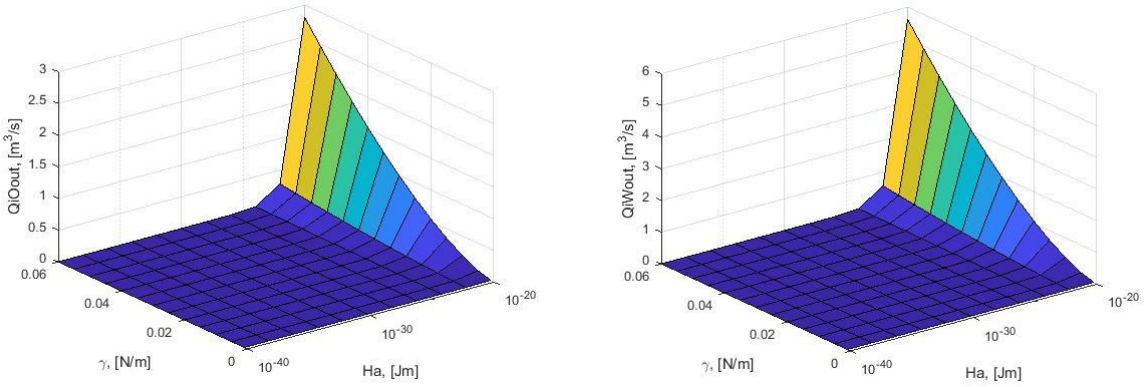

i. Oil Emulsion Phase ii. Water Emulsion Phase

Figure 5.1 b. Effect of Interfacial Tension and Hamaker Constant on Emulsion Outflow for Large Droplets

Observation of results presented in Figure (5.1a) and (5.1b) shows that the chosen limits for γ is always significant to the outflow, however Ha shows significance from approximately $1 \times 10^{-28}\ Jm$. Therefore, it would be reasonable to consider Ha from this value. However, from reported literatures, crude oil-water emulsion that is yet demulsified, have values of γ from $30 \times 10^{-3} - 32 \times 10^{-3}\ N/m$ and Ha of approximately $1 \times 10^{-30} - 1 \times 10^{-31}\ Jm$. Therefore, it would be reasonable to contract the limit for γ from about $5 \times 10^{-3} - 35 \times 10^{-3}\ N/m$ and consequently Ha from a value a little bit lower than $1 \times 10^{-28}\ Jm$. In addition, it is required to deduce reasonable, but yet practical pairings for γ and Ha. It is therefore important to have a guided range or starting point for theses pairings, and as earlier stated, crude oil-water emulsion with γ of $30 \times 10^{-3} - 32 \times 10^{-3}\ N/m$ correspond with Ha of approximately $1 \times 10^{-30} - 1 \times 10^{-31}\ Jm$. Assuming that the value of $30 \times 10^{-3}\ N/m$ is paired with $1 \times 10^{-30}\ Jm$, such that the values of Ha for the remaining values of γ $(i.e. 5, 10, 15, 20, 25\ and\ 35 \times 10^{-3}\ N/m\ )$ can be deduced via the trend or how the magnitude of incremental changes in Ha (resulting to a preassigned or pre-paired Ha) influence or collaborate with these values of γ. Suitable pairing would be based on how best it fits with the expectations of the current simulation case study. This approach has been adopted because γ - Ha pairings are rarely reported in literatures.

Therefore, based on advice from inhouse experts, suggesting that changes in γ of crude oil-water emulsion greatly affect Ha, an incremental change in the order of $1 \times 10^{-27}, 5 \times 10^{-28}, 1 \times 10^{-28}, \ldots, 1 \times 10^{-30}\ and\ 5 \times 10^{-31}\ Jm$ was initially proposed. Then an investigation of how the paired values of γ and Ha affect the product of the exponent of interfacial tension-retarded Hamaker constant, $GH = \gamma^{3/2} Ha^{1/2}$, as expressed in Equation (4.4) and emulsion outflows are shown in Figure(5.2a), (5.2b) and (5.2c) for minimum and maximum droplet radii.

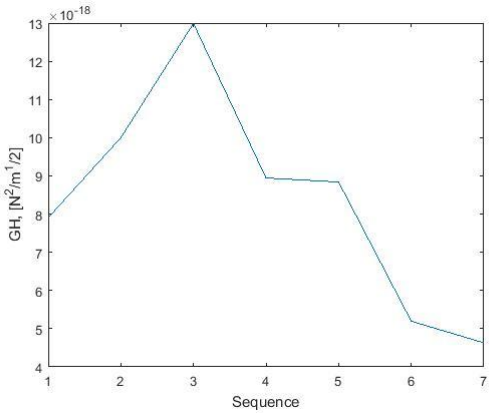

Figure 5.2 a. Trend of Hamaker constant

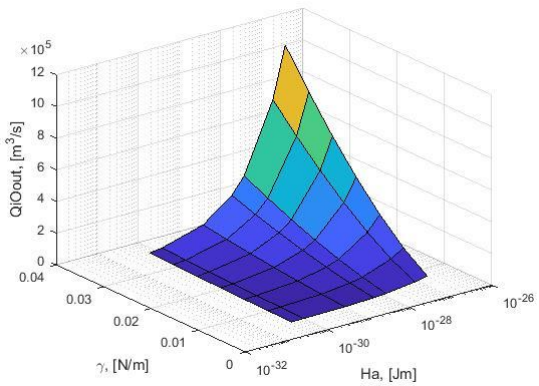

i. Oil emulsion phase

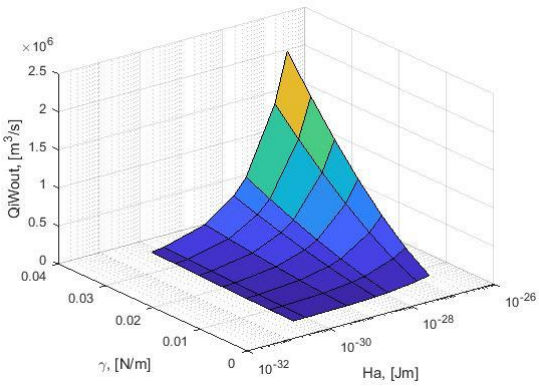

ii. Water emulsion phase

Figure 5.2 b. Effect of interfacial tension and Hamaker constant on emulsion outflow for small droplet

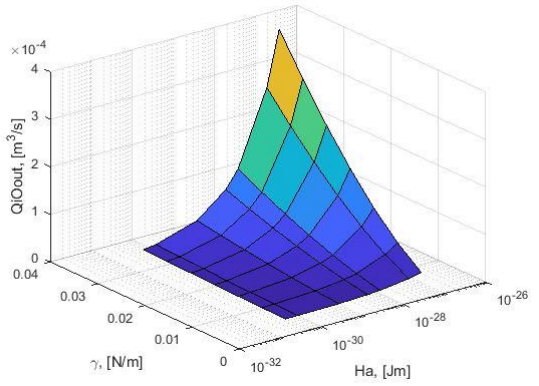

i. Oil emulsion phase

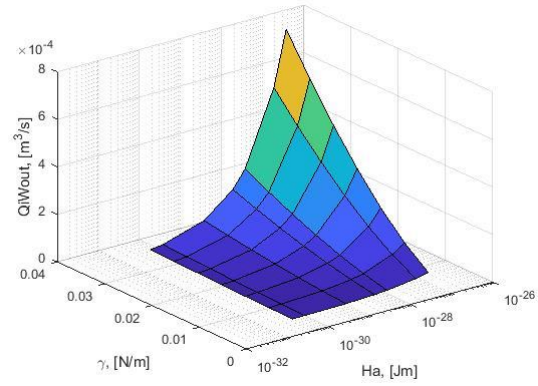

ii. Water emulsion phase

Figure 5.2 c. Effect of interfacial tension and Hamaker constant on emulsion outflow for large droplet

Observation of results from Figure (5.2a) shows an alternating contour, which is an indication that the outflow will dwindle with a change in Ha or γ. This is contrary to the expectation of this simulation case study, and therefore a likely indication of the fact that the proposed incremental change in Ha is incorrect, hence prompting further investigation with alternative incremental change.

Further investigation with an incremental change of Ha in the order of $1 \times 10^{-25}, 1 \times 10^{-26}, \ldots, 1 \times 10^{-30}$ and 1×10^{-31} , is considered with results shown in Figure (5.3a). Observation of these results show a somewhat steady trend. Although the incremental changes of Ha seem acceptable, the nominal factor of one (1) is not a practical value. Literature reports that nominal factors for Ha can range from 0.9 to 3.0 or more, based on this, a more reasonable nominal factor of 1.76 is chosen (Note that this is an arbitrary or empirical value just chosen other than using one). Therefore, this implies a more reasonable incremental change of Ha, in the order of $1.76 \times 10^{-25}, 1.76 \times 10^{-26}, \ldots, 1.76 \times 10^{-30}$ and 1.76×10^{-31} should be more appropriate. Result shown in Figure (5.3b) to Figure (5.3e) indicate that the outflow changes steadily with changes in Ha or γ . This is what is likely expected in practice, hence models best this simulation case study. However, it is important to buttress the fact that this incremental change or pairing is hypothetical and not experimentally based, hence may differ from what is expected in practice, and in other case scenarios. Therefore, it may also be possible in practice, that the incremental change can be in any of the following orders $(1 \times 10^{-20}, 5 \times 10^{-22}, \ldots, 1 \times 10^{-30}$ and 5×10^{-32} Jm), $(1 \times 10^{-25}, 1 \times 10^{-26}, 1 \times 10^{-27}, \ldots, 1 \times 10^{-30}$ and 1×10^{-31} Jm) or to even $(1 \times 10^{-27}, 5 \times 10^{-28}, 1 \times 10^{-28}, \ldots, 1 \times 10^{-30}$ and 5×10^{-31} Jm) etc.

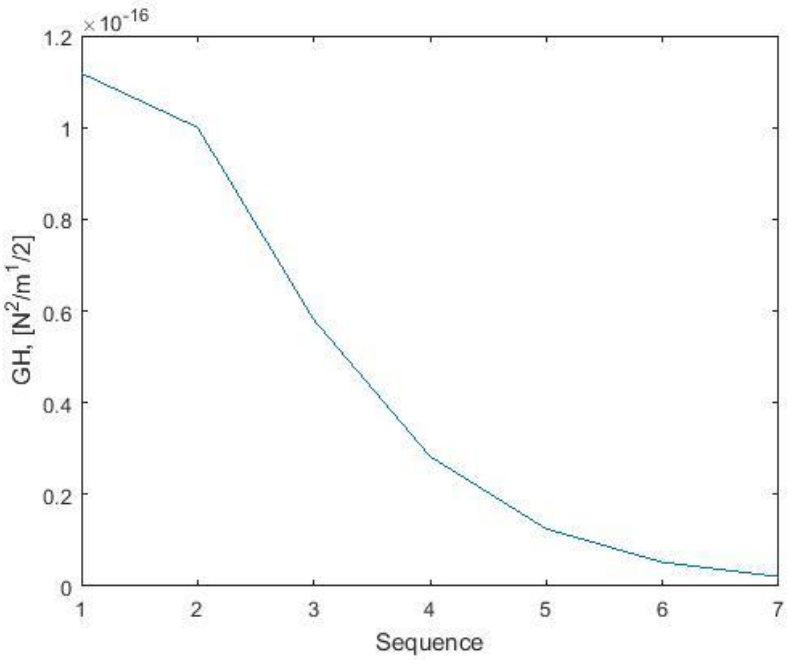

Figure 5.3 a. Trend of Hamaker constant

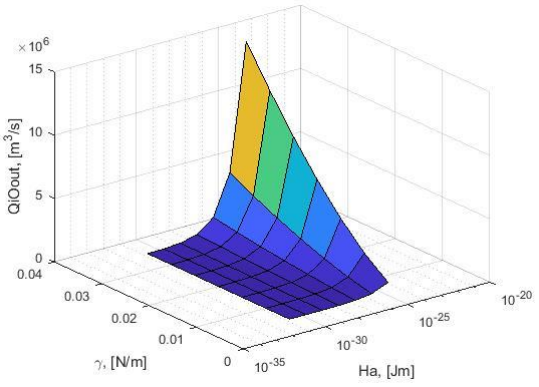

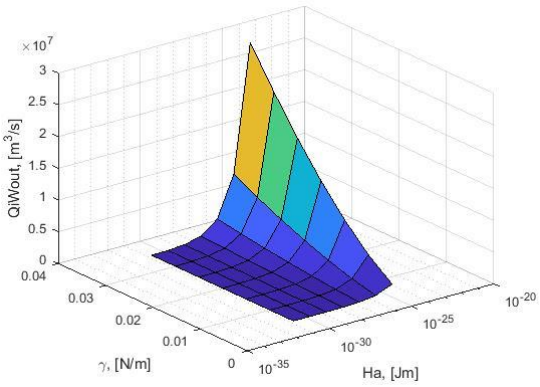

i. Oil emulsion phase ii. Water emulsion phase

Figure 5.3 b. Effect of interfacial tension and Hamaker constant on emulsion outflow for small droplet

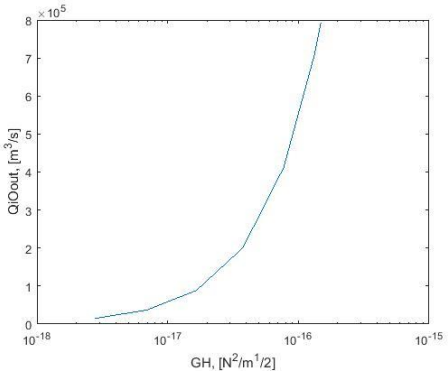

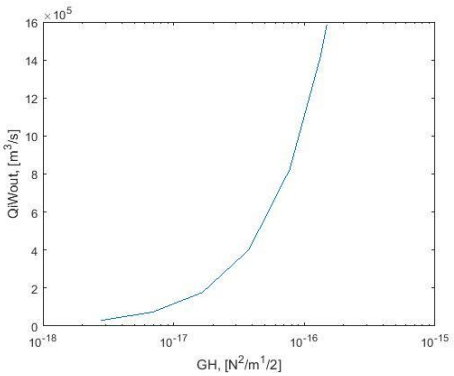

i. Oil emulsion phase ii. Water emulsion phase

Figure 5.3 c. Effect of exponential product of interfacial tension-Hamaker constant, GH on emulsion outflow for small droplet

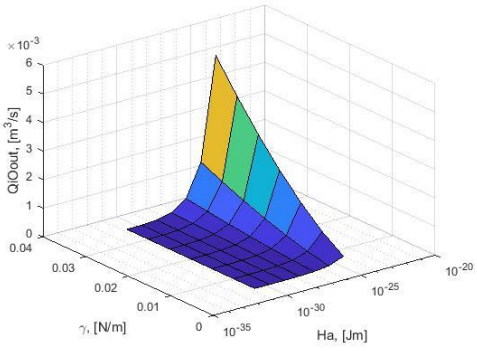

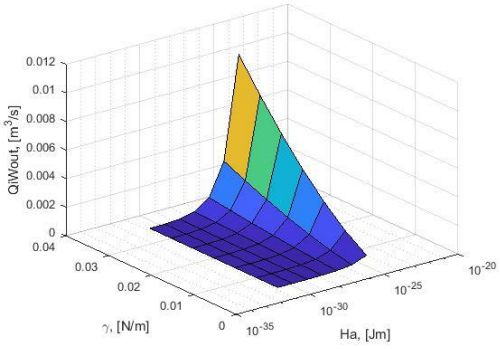

i. Oil emulsion phase ii. Water emulsion phase

Figure 5.3 d. Effect of interfacial tension and Hamaker constant on emulsion outflow for large droplet

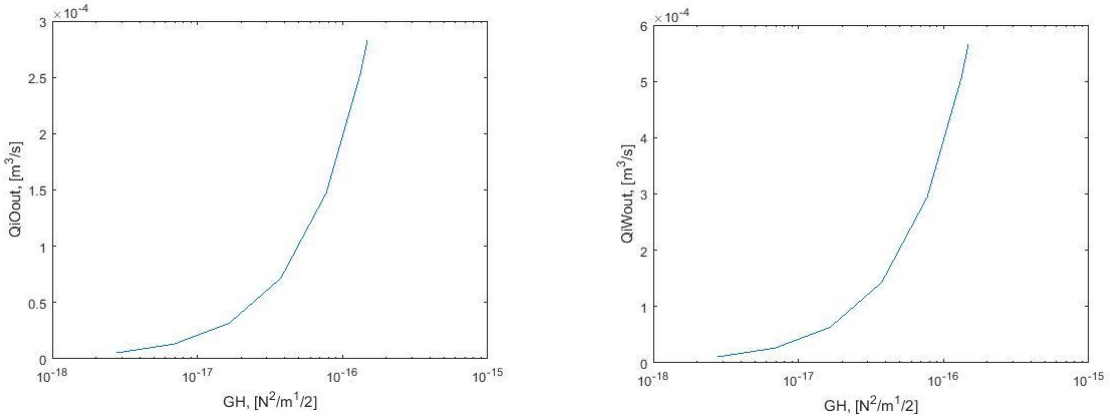

i. Oil emulsion phase ii. Water emulsion phase

Figure 5.3 e. Effect of exponential product of interfacial tension-Hamaker constant, GH on emulsion outflow for large droplet

Having deduced a satisfactory pairing for γ and Ha, a curved fitted relationship for γ and Ha is deduced as shown in Equation (5.1) based on the simulation result and in collaboration with the relationship from M.K. Chaudhury (Chaudhury, 1987) for surface tension and Hamaker constant ($H/\gamma^* = 1.86(\pm 0.16) \times 10^{-14}\ cm^2$).

$$Ha = \gamma 1.7564 \times 10^{(-20-(\gamma/\gamma_{\min}))} \times \ln(1 + (0.0001/\gamma)) \tag{5.1}$$

Basically, this curve fitted equation is a product of γ, a nominal factor, a power function and a logarithmic function, with the functions in terms of γ. The nominal factor, 1.7564 represent a constant value, such that when multiplied by γ gives typical nominal factor of Ha such as 0.9×10^{-power}, 1.27×10^{-power}, etc. as reported in literature, (Silva, et al., 2013). While the power function, $10^{(-20-(\gamma/\gamma_{\min}))}$ serves to incorporate the exponential changes in Ha, as γ changes, however this part of the power function is best fitted for γ within the range of $10 \times 10^{-3} - 35 \times 10^{-3}\ N/m$, and not for γ less than $10 \times 10^{-3}\ N/m$. Therefore, in order to improve the fit, a logarithmic part, $\ln(1 + (0.0001/\gamma))$ is introduced. This logarithmic function acts to normalize values to γ below and above $10 \times 10^{-3} N/m$ such that the fitted equation yields a steady exponential trend. This implies that utilizing logarithmic function, it is reasonably accurate to use the curve fitted equation for γ below $5 \times 10^{-3}\ N/m$. However, it should be noted that the further below, the less accurate the result. A comparison of test data for Ha and a curve fitted equation for Ha is shown in Figure (5.4).

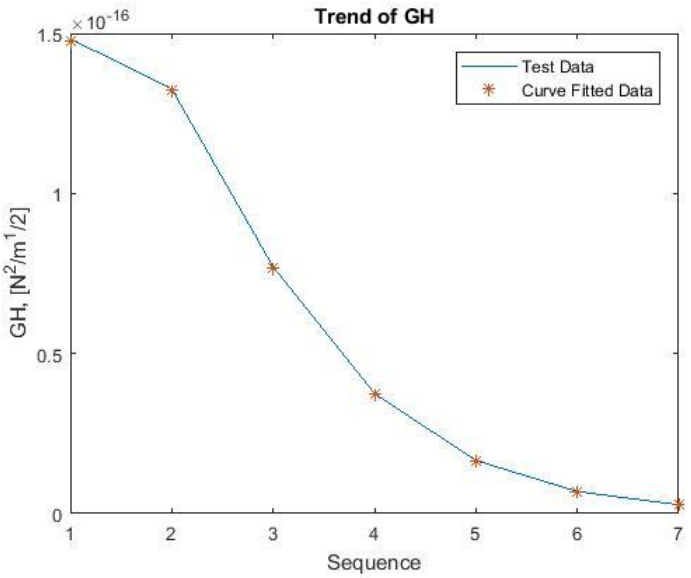

Figure 5.4 1. Comparison of test data and curve fitted equation for Ha via GH plotting

5.2 Droplet Size Evaluation

The next course of action, is to investigate and narrow the droplet sizes, which closely fit the desired outflow range expected for this simulation model. This can be achieved by plotting GH together with droplet sizes ranging from $1 - 500\mu m$ for both water and oil, using an incremental change in radius of $20\mu m$. Results shown in Figure (5.5a) and (5.5b) suggest that small radii lead to very large flowrates beyond the limit of this simulation case study. Hence contrasting the investigation boundary to say $130 - 430\mu m$ for the water phase and $80 - 400\mu m$ for the oil emulsion phase, while using a smaller incremental change of $10\mu m$, helps to narrow the simulation results to the expected boundary. Based on this, hypothetical droplet radii suitable for this simulation model are found to be approximately $110\mu m$ for water and $90\mu m$ for oil emulsion phase, respectively.

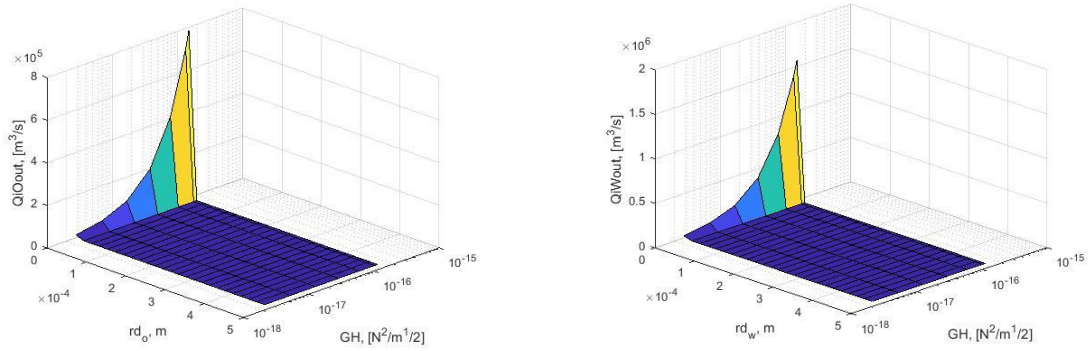

i. Oil emulsion phase ii. Water emulsion phase

Figure 5.5 a. Initial investigation of effect of droplet radius on emulsion outflow at paired interfacial tension and Hamaker constant

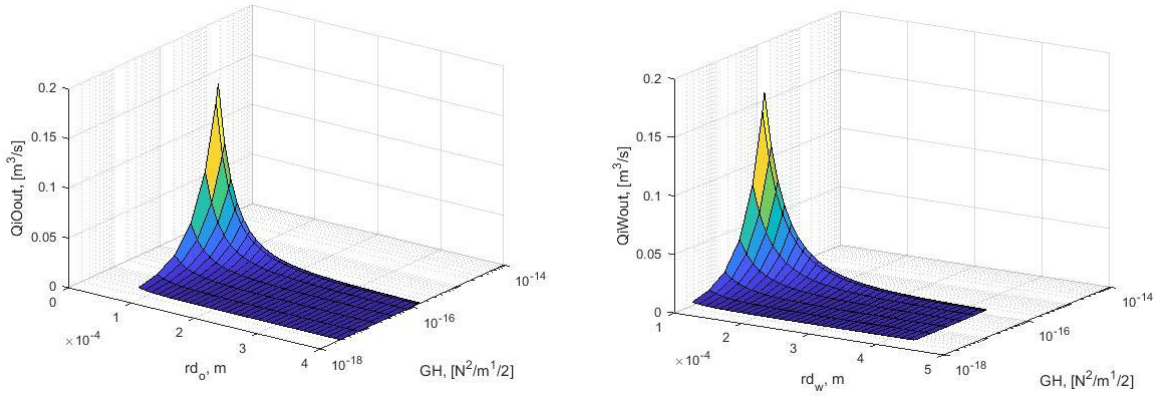

i. Oil emulsion phase ii. Water emulsion phase

Figure 5.5 b. Contracted investigation of effect of droplet radius on emulsion outflow at paired interfacial tension and Hamaker constant

The hypothetical droplet sizes, D_p,can be related to a somewhat practical, D and empirical droplet size, D_E (given in Equation (2.4)). These values are expected for this simulation case study and other simulation cases in general by expressing D_p to D or D_E via correction factors, K or K_{re} as given in Equation (5.2) and (5.3). The correction factor would most likely, be unique for a given case model.

$$D_E = K_{re} \times D_p \tag{5.2}$$

$$D = K_r \times D_p \tag{5.3}$$

Where, $D_p = 2r_p$, is the simulated droplet size

In summary, the objective of this chapter involved the deduction of Equation (5.1) and optimal hypothetical droplet radii of approximately $110\mu m$ for water and $90\mu m$ oil emulsion phase.

Chapter 6

6 Flushing of Emulsion

Flushing involves washing off of the oil phase and oil-water interface from the gravity separation via a rising water phase. Flushing is initiated when the water level approaches the weir height of the gravity separator. This is operationally achieved by shutting off the water outlet valve, while the inlet valve as well as the oil and gas outlet valves remain open.

Flushing is not a frequent method of handling growing emulsion layers. It is implemented when the use of demulsifiers is no longer economically viable or when the rate of emulsification is beyond the capacity the available demulsifier can handle. Uncontrollable emulsification is not a frequent phenomenon during well production. Therefore, flushing is a periodic or emergent method of handling crude emulsions.

Flushing is a time dependent process, and this is because it is solely dependent on the magnitude of the oil outflow. Since the outlet valve for water is shut, flushing is therefore achieved via adjustment of oil outflow to an optimal magnitude.

The following conditions hold for flushing:

1. Water level,h_W approaches the weir height, h_{weir} of the gravity separator

$$h_W = h_{weir}$$

2. The flushing time,t_{flu} is logically required to be greater or equal the residence time, t_{res}, so as to ensure emulsion layers are fully developed, and hence completely discharged.

$$t_{flu} \geq t_{res}$$

Since these conditions are predominately dependent on oil outflow, $q_{O,out}$. Specifically, to achieve the second condition, the magnitude of $q_{O,out}$ is methodically adjusted via a flushing factor, K_{flu}. Where, $K_{flu} \leq 1$

$$K_{flu} q_{O,out} = q_{O,out,flu}$$

Chapter 7

7 Control of Emulsion layer

As earlier alighted, a very important component of the gravity separator is the pressure and liquid-level controller. The pressure of gravity separators is maintained by a pressure controller, using the gas outflow as manipulated variable. In practice this is achieved by prompting the valve of the gas open (when accumulated gas exceed design limit) or close (when accumulated gas is below design limit) (Wang & Economides, 2009). Similarly, liquid level is controlled to prevent flooding. This is achieved by prompting open the outlet valves for water and oil phases. The consideration of emulsion layer as a phase makes the system complex. This is because the inhomogeneity, opacity, and multitude of phases that exist in emulsion layers. Therefore, measurement requires the use of very sensitive and often expensive devices. These devices are generally classified as radioactive or non-radioactive types, and they feature one or more of the following abilities: They are non-intrusive and non-invasive; They can operate continuously and require minimum maintenance; They are intrinsically safe and can operate in zone zero areas; They can be a clamp-on type and externally mounted (Meribout, et al., 2011). Typical examples of theses device include:

1. Differential pressure-based device
2. Capacitive sensor-based device
3. Radar or microwave-based device
4. Radiation-based device
5. Vibrating switches-based device
6. Optical fibre-based device
7. Ultrasonic-based device

Presently, from the accuracy point of view, radioactive-based devices seem to be the most successful devices. However, because of the danger it poses to operators, an alternative safe solution is the use of ultrasonic sensors.

7.1 Control system- Feedback control

In general, control systems involve the interconnection of the various components of a system to form a configuration that will provide a desired system response. The most important component of a control system is its input and output. This is because input-output relationship represents the cause-and-effect relationship of the process, and based on this relationship, a control system can be classified as: Open-loop control system (system that utilizes a controller or control actuator to obtain the desired response, without using a feedback); Closed-loop control system (system that utilizes an additional measure of the actual output (feedback signal) to compare with the desired output response) (Dorf & Bishop, 2008). In industrial control, feedback control system is commonly used because it uses very simple technique, effectiveness for many disturbances, provides zero offset, and works with minimum knowledge of the process (Skogestad, 2018). Shown in Figure (7.1) is a feedback control system.

Chapter 7

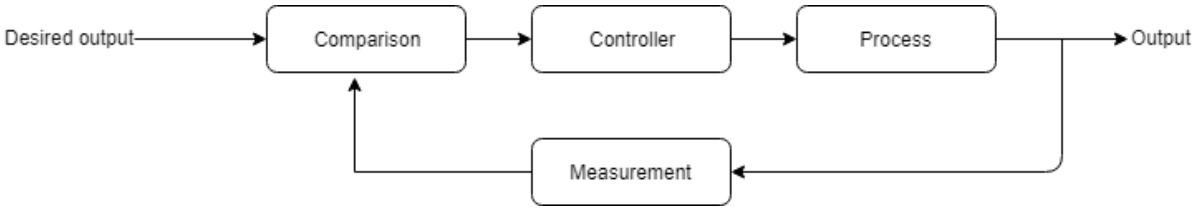

Figure 7. 1. Feedback control system

7.2 Feedback-Basic Control Mode

There are three basic control modes that can be used to implement a feedback control system and they include: Proportional control, Integral control and derivative control mode. These control modes are usually used in single or combination state. The most commonly used are Proportional, Proportional-Integral and Proportional-Integral-Derivative control mode.

7.2.1 Proportional Control

Proportional control in feedback control, is primarily used to reduce the error signal, $e(t)$. The error signal is given in Equation (7.1).

$$e(t) = y_{sp}(t) - y_m(t) \tag{7.1}$$

Where,$y_{sp}(t)$, is the setpoint and $y_m(t)$ is the measured value of the controlled variable. The expression given by Equation (7.1) indicates $y_{sp}(t)$ is time-varying, in practice however this is kept constant over a range of time. Therefore, the controller output, $P(t)$ is proportional to $e(t)$, as given in Equation (7.2).

$$P(t) = \bar{P} + K_c e(t) \tag{7.2}$$

Where,$\bar{P}$ is the bias value for a steady state system and K_c, is the controller gain for the system. The drawback of pure proportional controllers is that they tend to have an offset and typically cannot bring the error signal to zero. Therefore, the addition of integral action is required ensuring the error signal converging to zero.

7.2.2 Integral Control (Proportional-Integral Control)

In Integral control mode, the controller output depends on the integral of the error signal over time. Therefore, the controller output, $P(t)$ is proportional to the integral of the control error, $\int_0^t e(t)dt$, as given in Equation (7.3).

$$P(t) = \bar{P} + \frac{1}{\tau_I}\int_0^t e(t)dt \tag{7.3}$$

Integral control is not used alone as it is usually used in conjunction with proportional control to form proportional-integral (PI) controller. The integral control element of the controller eliminates offset that might be caused by the proportional element. Therefore, in this case the controller output, $P(t)$ is as given in Equation (7.4).

$$P(t) = \bar{P} + K_c\left(e(t) + \frac{1}{\tau_I}\int_0^t e(t)dt\right) \tag{7.4}$$

Where, τ_I is an adjustable parameter referred to as the integral time. It should however be noted that the inherent disadvantage of integral control action is a phenomenon known as reset windup or integral windup, which is a situation where the controller operates beyond limit of the manipulative variable, when large change in the setpoint occur. Anti-windup solutions exist that prevent the controller from integrating further even when the signal is saturated. The Laplace transformation of Equation (7.4) is expressed in Equation (7.5).

$$C(s) = K_c\left(1 + \frac{1}{\tau_I s}\right) \tag{7.5}$$

7.2.3 Derivative Control (Proportional- Integral-Derivative Control)

The function of derivative control action is to anticipate the future behaviour of the error signal by considering its rate of change. Therefore $P(t)$ is proportional to the derivative of the control error, $de(t)/dt$ as given in Equation (7.6).

$$P(t) = \bar{P} + \tau_D\frac{de(t)}{dt} \tag{7.6}$$

Where, τ_D is the derivative time. Anticipatory strategy is usually incorporated in automatic controllers by making the controller output proportional to the rate of change of the error signal or the controlled variable. The derivative term usually includes a derivative mode filter (also called a derivative filter) that reduces the sensitivity of the control calculations to high-frequency noise in the measurement.

Derivative control is typically not used alone as it is used in conjunction with proportional-integral (PI) control mode to yield proportional-integral-derivative (PID) control mode as given in Equation (7.7).

$$P(t) = \bar{P} + K_c\left(e(t) + \frac{1}{\tau_I}\int_0^t e(t)dt + \tau_D\frac{de(t)}{dt}\right) \tag{7.7}$$

The Laplace transformation of Equation (7.7) can be expressed as given in Equation (7.8).

$$C(s) = K_c\left(1 + \frac{1}{\tau_I s} + \tau_D s\right) \tag{7.8}$$

7.3 Controller Design and Tuning

Controller design and tuning is a mandatory task often required during the initialization of a process plant, and in most cases, this can be a challenge to operators without knowledge in controller tuning. A simple and yet effective controller tuning method, which has been widely used in industry is the "Skogestad Internal Model Control" method for PID controller tuning. This method is popularly known as the SIMC rule (Skogestad, 2003).

7.3.1 SIMC Tuning Rule

The SIMC tuning for PID controller of a second order system is as given in Equation (7.9) -(7.11).

$$K_c = \frac{1}{K'(\theta^* + \tau_c)} \tag{7.9}$$

$$\tau_I = \min\left(\tau_1, 4(\tau_c + \theta^*)\right) \tag{7.10}$$

$$\tau_D = \tau_2 \tag{7.11}$$

However, for first order system, which are best controlled via a PI controller, τ_D, is zero. The other parameters in Equation (7.9) -(7.11) are defined or deduced graphically as shown in Figure (7.2).

where the parameters in Equation (7.9) -(7.11) can be expressed or used as, $K' = K/\tau_1$ and the tuning time constant, $\tau_c \geq \theta$ ($\tau_c = \theta^*$, for tight control and $\tau_c > \theta^*$, for smooth control). Note that, θ^*, is the delay in response signal.

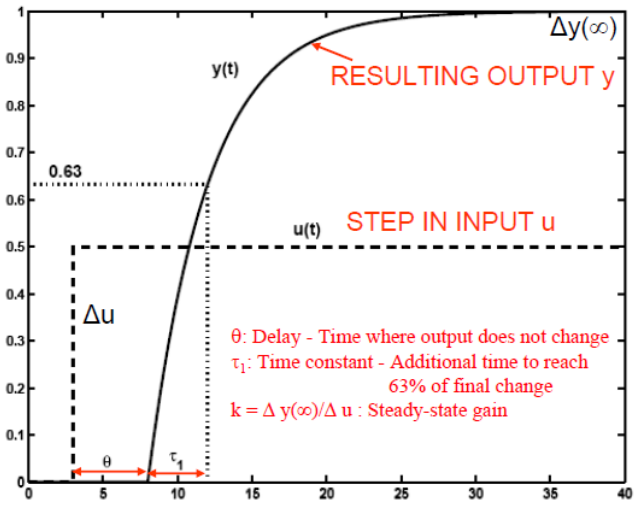

Figure 7. 2. Graphical deduction of tuning parameter for first order system (Skogestad & Grimholt, 2011).

The SIMC tuning for integrating system controlled by PI controller is tuned a little differently. A graphical illustration of essential parameters required for tuning are shown in Figure (7.3).

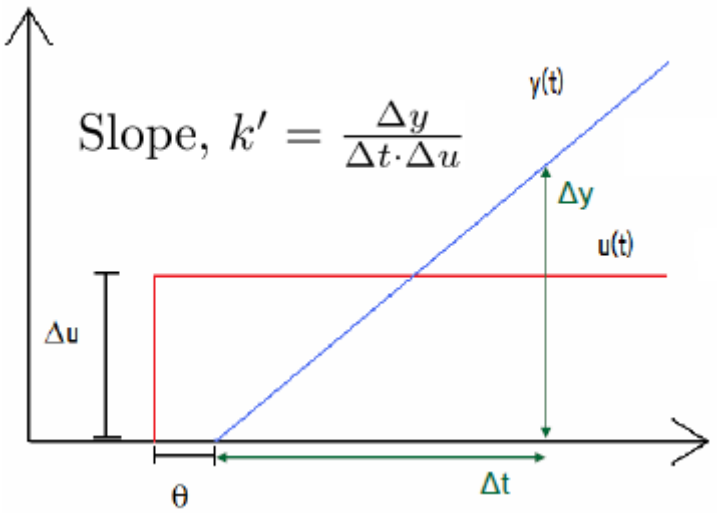

Figure 7. 3. Graphical deduction of tuning parameter for integrating system (Skogestad & Grimholt, 2011).

Chapter 8

8 Procedures in deducing the tuning parameters

Using data for well production of the reservoir at a time regime approaching the end of its lifetime, as basis, the following sequential steps were performed.

1. The steady state value of the manipulative variable (interfacial tension for both oil, $\gamma_{iO,ss}$ and water, $\gamma_{iW,ss}$ interface) are deduced independently. i.e. the values of $\gamma_{iO,ss}$ at which $dV_{iO}/dt \cong 0$ (hence $h_{iO} = 0$)and $\gamma_{iW,ss}$ at $dV_{iW}/dt \cong 0$ (hence $h_{iW} = 0$).

Considering the oil-interface:

$$\frac{dV_{iO}}{dt} = \frac{V_{OoW}}{V_O} q_{L,in}(\beta \emptyset_{OW}) - q_{iO,out} = 0$$

Where $q_{iO,out}$ can be computed by combining Equation (4.3) and (4.4) yields:

$$\frac{V_{OoW}}{V_O} q_{L,in}(\beta \emptyset_{OW}) - \frac{A_i r_d \gamma_{iO,ss}^{3/2} Ha^{1/2}}{3.138 \mu_c (\rho_d - \rho_c) g_z r_d^{7/2}} = 0$$

Considering water-interface:

$$\frac{dV_{iW}}{dt} = \frac{V_{WoO}}{V_W} q_{L,in}(\alpha \emptyset_{WO}) - q_{iW,out} = 0$$

similarly, $q_{iW,out}$ can be computed in same way as $q_{iO,out}$ to yields

$$\frac{V_{WoO}}{V_W} q_{L,in}(\alpha \emptyset_{WO}) - \frac{A_i r_d \gamma_{iW,ss}^{3/2} Ha^{1/2}}{3.138 \mu_c (\rho_d - \rho_c) g_z r_d^{7/2}} = 0$$

The values for $\gamma_{iW,ss}$ and $\gamma_{iO,ss}$ is deducible from simulation, as illustrated in Figure (8.1) and given in Table (8.1).

2. A step change in the manipulative variable (interfacial tension, γ) from steady state value (for example a change to $25 \times 10^{-3} N/m$) is deduced at open loop (i.e. without controllers) at a time fraction of the complete simulation time (for example 100 seconds). This gives $\Delta\gamma_i$ as shown in Table (8.1).

3. The change in response, Δh_i and time for observable difference in response, Δt (i.e. difference in complete simulation time and time for step change in interfacial tension ($\Delta\gamma$)) can be deduced from Figure (8.2).

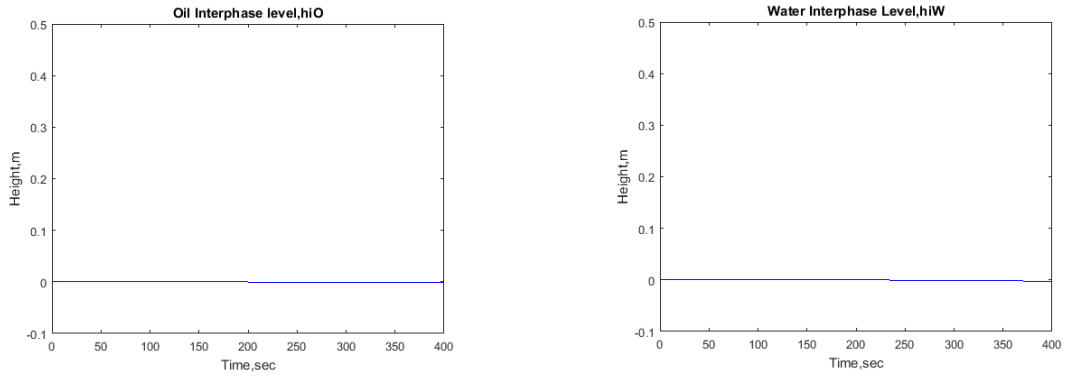

i. Oil Emulsion Level ii. Water Emulsion Level

Figure 8. 1. Computation from simulation to deduce $\gamma_{iO,ss}$ and $\gamma_{iW,ss}$ at h_{iO} and h_{iW} approximately zero

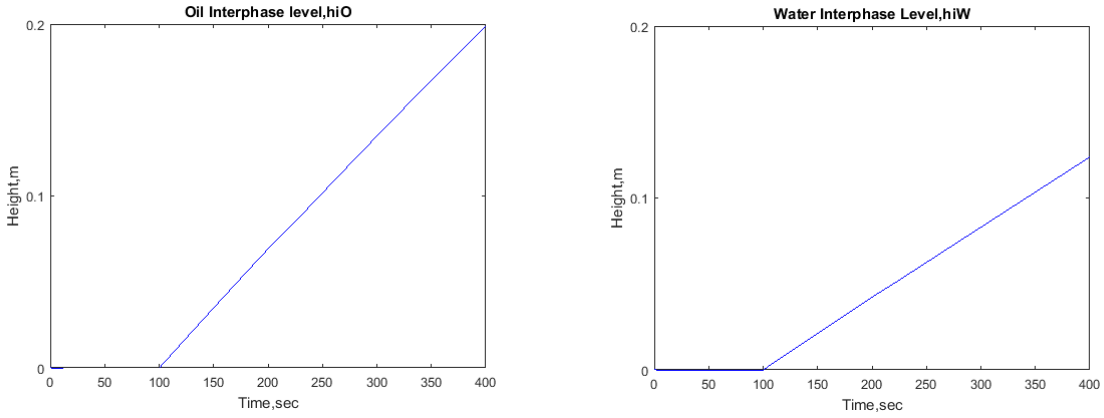

i. Oil Emulsion Level ii. Water Emulsion Level

Figure 8. 2. Response of h_{iO} and h_{iW} to step change in $\gamma_{iO,ss}$ and $\gamma_{iW,ss}$

The system shown in Figure (8.2) resembles that of Figure (7.3), the only difference being that the process is without delay. There is no delay in demulsification because at the chosen time of 100seconds

for step change in interfacial tension there is an immediate response in the interfacial level as shown in Figure (8.2).

The tuning parameters are deduced as illustrated in step (1) to (3):

$$K' = \frac{\Delta h_i}{\Delta\gamma\Delta t} \qquad \text{(step.1)}$$

$$K_c = \frac{1}{K'(\theta^* + \tau_c)} \cong \left(\frac{1}{K'\tau_c}\right)_{\theta\to 0} \qquad \text{(step.2)}$$

$$\tau_I = \min\left(\tau_1, 4(\tau_c + \theta^*)\right) \cong (4\tau_c)_{\theta^*\to 0} \qquad \text{(step.3)}$$

The computed values in step (1) to (3) can then be substituted into Equation (7.5). However, PI controller in MATLAB takes the form as shown in Equation (8.1).

$$C(s)_{matlab} = K_p + \frac{T_I}{s} \qquad (8.1)$$

Where, $K_p = K_c$ and $T_I = K_c/\tau_I$. The value of τ_c is then fixed, based on how fast the system is to be controlled and also experience with the system. Tuning parameters for the emulsion demulsification process is given in Table (8.1).

Table 8. 1. Computed tuning parameters for controlling water and oil interface

Parameters for Controller	Water Interface	Oil-Interface
$\gamma_{i,ss}$	18.5800×10^{-3}	20.4900×10^{-3}
γ_i	25.000×10^{-3}	25.000×10^{-3}
$\Delta\gamma_i, N/m$	6.42×10^{-3}	4.51×10^{-3}
$\Delta h_i, m$	0.1987	0.1238
$\Delta t, sec$	300.0000	300.0000
K'	0.1032	0.0915
$K_c = K_p$	$9.6930/\tau_c$	$10.9289/\tau_c$
τ_I	$4\tau_c$	$4\tau_c$
T_I	$K_c/4\tau_c$	$K_c/4{\tau_c}^2$
τ_c	5.0000	5.0000

These parameter in Table 8.1, together with the desired response (i.e. level of the interface) serve as inputs for the PI controllers for the water and oil interface. Note that these controller tuning parameters were deduced on the basis of well production, when the reservoir is approaching the end of its lifetime.

Chapter 9

9 Result and Discussion

This section presents results from simulation (via MATLAB scripts and SIMULINK) of model equations and parameters deduced from chapters 2 to 8. The dimension of separator used in simulation are 1.65m radius, 2m weir height and 10m active separation zone. Also, additional thermodynamic fluid properties required are given in the Table (9.1).

Table 9. 1. Thermodynamic fluid properties for simulation

Parameters	Description	Value	Unit
R	Ideal Gas Constant	8.31	$m^3 Pa mol^{-1} K^{-1}$
T	Temperature of Fluid	328.5	$Kelvins$
ρ_g	Density of gas	49.7	kg/m^3
ρ_O	Density of Oil	831.5	kg/m^3
ρ_W	Density of Water	1030	kg/m^3
M_G	Molar Mass of gas	0.01604	$kg/moles$
μ_O	Viscosity of Oil	0.5e-3	$Pa.sec$
μ_W	Viscosity of Water	1e-3	$Pa.sec$

Initialization parameters for simulation, are given in Table (9.2).

Table 9. 2. Initial values for the integrators of the dynamic states

Parameters	Description	Value	Unit
$h_{L,init}$	Initial value for the liquid level	2.5	m
$h_{W,init}$	Initial value for the water level	1.4	m
$h_{iO,init}$	Initial value for the Oil interface level	0.1	m
$h_{iW,init}$	Initial value for the Water interface level	0.1	m
P_{init}	Initial pressure	68.7	bar
Initial separation efficiencies in the inlet zone of the separator (Perfect separation for $\emptyset = 0$)			
$\emptyset_{wo}$	Fraction of water into continuous oil phase	0.3	–
$\emptyset_{ow}$	Fraction of oil into continuous water phase	0.3	–

Analysis of separator performance will involve consideration of two main simulation case studies: Well production in beginning of the reservoir lifetime and towards the end of the reservoir lifetime, with each case simulated for conditions when there is no force induced interfacial outflow (i.e. water interface output,q_{iWout} and oil interface output,q_{iOout}), and when there is force induced interfacial outflow (to control the emulsion layer).

Chapter 9

9.1 Simulation of gravity separator at the beginning of reservoir lifetime

During well production at the beginning of reservoir lifetime, oil cut in input stream to the horizontal separator is at its highest and data for this stage of production are given in Table (9.3).

Table 9. 3. Data for simulation at the beginning of the reservoir lifetime

Parameters	Description	Value	Unit
α	Water Cut	0.135	–
β	Oil Cut	0.865	–
q_{Lin}	Inlet Volumetric Flowrate of Liquid	0.59	m^3/s
q_{Gin}	Inlet Volumetric Flowrate of Gas	0.456	m^3/s

9.1.1 Conditions with no force induced interfacial outflow

Results shown in Figure (9.1) - (9.5) are deduced for condition when there is no forced induced interfacial outflow from emulsion layers to respective continuous phases. These results have been optimally analysed for a duration of 400 seconds.

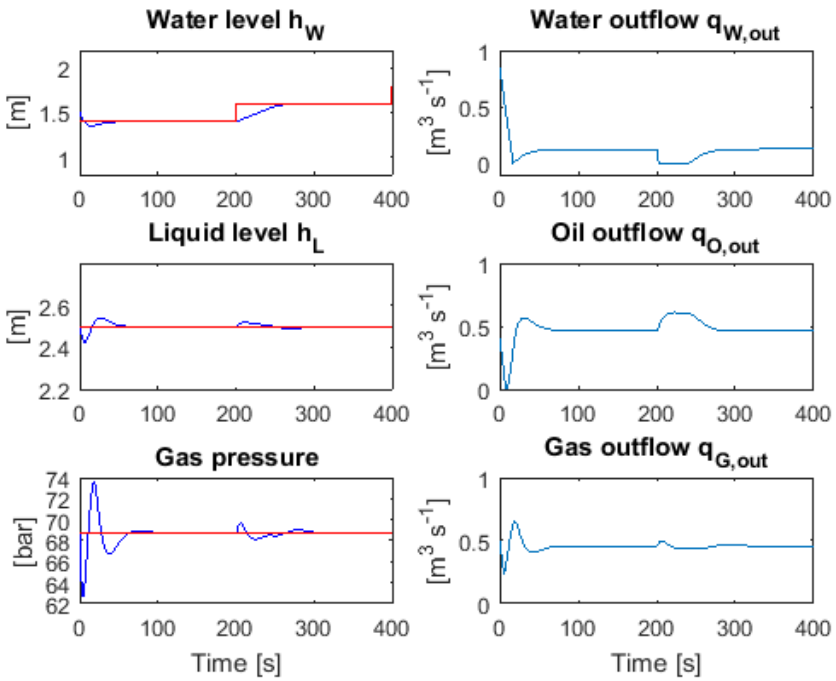

Figure 9. 1. Relationship of fluid outflow with respect to their set level or pressure-part (1a)

Chapter 9

Based on simplicity in the model development, steady state operation of the liquid phase has been assumed. This has been implemented via a liquid level controller to ensure that liquid level, h_L remains constant at $2.5m$, as shown in subplot (3,2,3) in Figure (9.1). Furthermore, the water level,h_W in subplot (3,2,1) is kept reasonably within the step changes in the setpoint of $1.4m$ and $1.6m$ as inputted to the water level controller.

At the initial time of separation, input stream to the separator initially segregate into gas and liquid phase. The liquid phase constitutes of water and oil phase, so that, $h_L = h_W + h_O$.Then as separation time approaches the designed residence time, oil and water interface develops out of the water and oil phase leaving behind a continuous water and oil phases respectively. However, the volume of the water (continuous water + oil interface) and oil (continuous oil + water interface) phase remains constant. However, since the liquid phase is expected to remain at steady state, it implies that if the water level increases the oil level decreases vice versa. Furthermore, it implies that if the oil or water interface layers grow larger, the water or oil continuous phases grow smaller vice versa.

In analysing the concepts discussed so far in relation to volumetric flowrate, it can be inferred that as the volumes of the continuous phases decrease (i.e. interfaces increase), lesser inflowing water or oil from the feed stream will be retained in the separator or higher impure water or oil will be discharged from the separator, vice versa. But it should be noted that both water and oil phase in the separator cannot increase at the same time. i.e. if the volume of the water phase decreases, the oil phase will consequentially increase. Furthermore, since the volume of these phases can only be controlled via their output, decreasing (e.g. oil phase) or increasing (e.g. water phase) volume of one phases in the separator implies a corresponding increase (oil phase, q_{Oout}) or decrease (water phase, q_{Wout}) outflow from the separator. This is illustrated in the first 50 seconds and between 200-240 seconds of Figure (9.1), subplot (3,2,2) and (3,2,4). While in a situation, when the volume of these phases in the separator are kept constant (via response to a controller), their corresponding outflow is expected to be constant as shown between 241-400 seconds of the above figure, subplot (3,2,2) and (3,2,4).

Finally, in respect to Figure (9.1), since the level of the liquid phase, h_L is held constant at $2.5m$, the pressure of gas is expected to remain constant as shown in subplot (3,2,5). Consequentially this means the gas outflow is constant as shown in subplot (3,2,6), in accord with the universal gas law.

Now considering Figure (9.2), comparison of subplot (1,3,1), subplot (3,3,2) and subplot (3,3,3) validate that the liquid phase constitutes of water and oil phase, since it can be clearly seen that $h_L = h_W + h_O$, as expected. It can also be observed that in the same manner the water level, h_W increases from 1.5m to 1.6m so does the oil level, h_O correspondingly decreases from 1m to 0.9m

Also, further observation of subplot (3,3,2), subplot (3,3,5) and subplot (3,3,8) validate the assumption that, $h_W = h_{WC} + h_{iO}$. It can be also observed that as oil interface, h_{iO} grows, the water continuous phase, h_{WC} correspondingly decreases. Similarly, observation of subplot (3,3,3), subplot (3,3,6) and subplot (3,3,9) also validate that, $h_O = h_{OC} + h_{iW}$, however the rate at which the water interface grows (from 0.1m to approximately 0.1076m) is slower compared to the growth of oil interface (from 0.1m to 0.6725m). This is expected, because not much water is dispersed in the oil phase as opposed to oil dispersion in water.

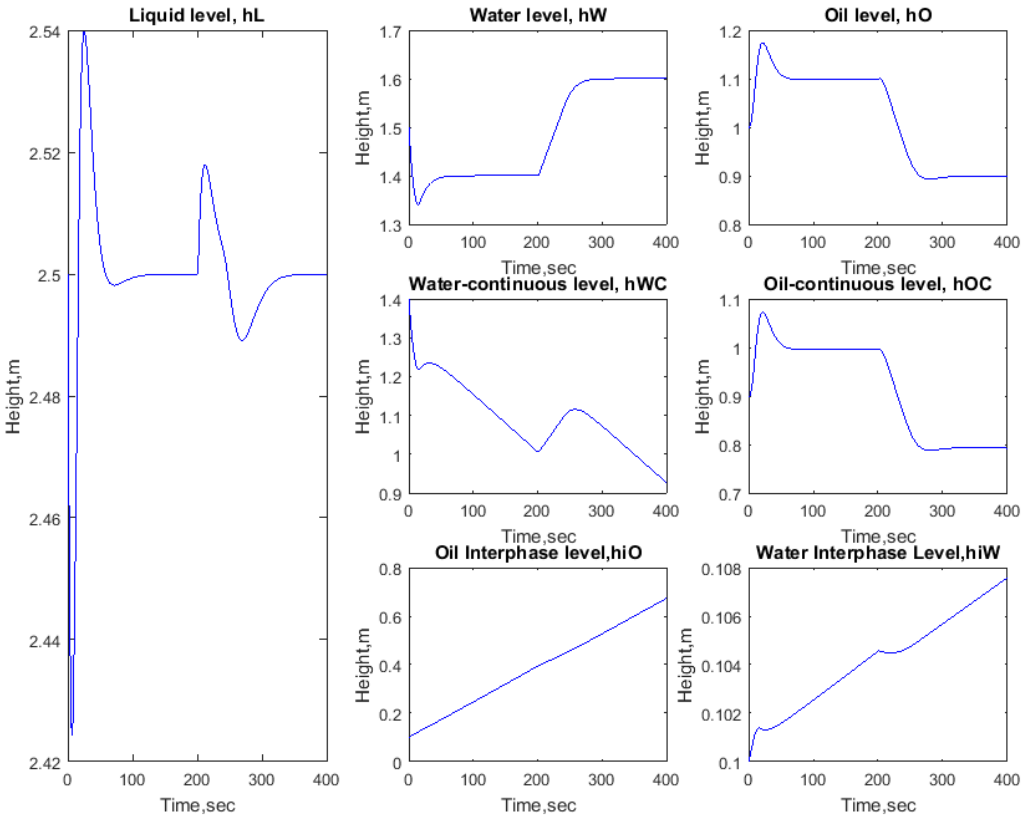

Figure 9. 2. Levels of various composition of the liquid phase with respect to time-Part (1a)

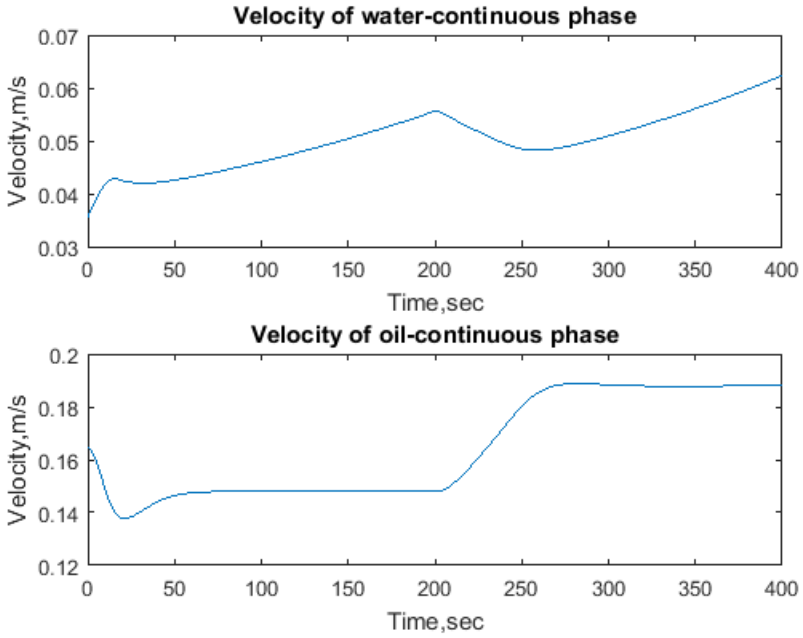

Figure 9. 3. Velocity profile for continuous phases-Part (1)

The Figure (9.3) shows that the velocity for water and oil continuous phases increasing with time. This is the outcome expected because as the respective interfaces grows, the volume of the continuous phases decreases. Therefore, at constant flow rate, velocities of the continuous phases will increase. However, the velocity of the water continuous phase increases more rapidly because the oil interface grows more rapidly, and as such the volume of the water continuous phase correspondingly decreases rapidly.

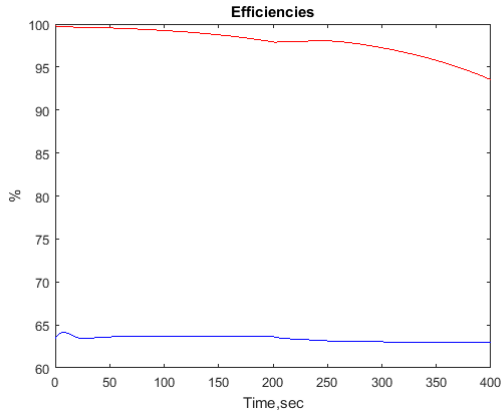

Figure 9. 4. Efficiencies of removal of oil from water (red) and water from oil (blue) over time- Part (1)

In consideration to Figure (9.4), based on earlier validation that oil interface grows rapidly from the water phase, which result to smaller volume of the water continuous phase in the separator. Therefore, much of the water being fed to the separator will be consequentially discharged rapidly. Higher outflow of water, implies that the residence time of water stream is less than the designed limit. This consequently results in poorer separation of the water phase into pure water continuous phase. This situation is illustrated via the red curve, which indicates an observable decrease from approximately 99.5% to about 94% in separation efficiency for the water phase. However, observation of the blue curve indicates that the separation efficiency of oil is almost steady at 63%. This is an indication that water interface grows very slowly from the oil interface or lesser droplets of water are dispersed in oil. Note that efficiency indicates how much of the dispersed oil or water could be removed from the respective continuous phases

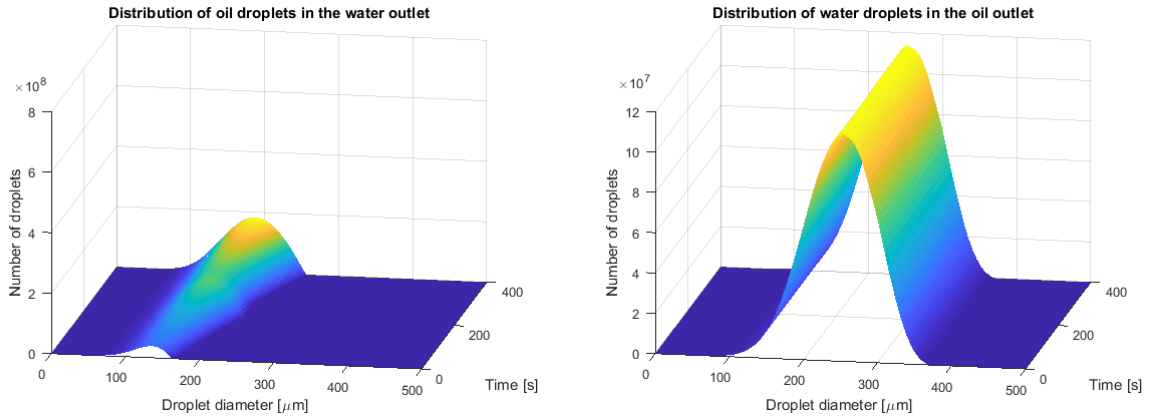

i. Distribution of oil droplets in the water Outlet ii. Distribution of water droplets in the oil outlet

Figure 9. 5. Distribution of disperse phase in continuous phase-Part (1)

The Figure (9.5), correspond directly to the efficiency plots, Figure (9.4). The distribution of water droplets in the oil outlet is almost constant with time and as such evenly distributed as shown in Figure (9.5-ii), as opposed to oil distribution in water as illustrated in Figure (9.5-i).

9.1.2 Conditions with forced induce interfacial outflow via demulsifier

Results shown in Figure (9.6) - (9.11) are deduced for condition when the demulsifier forcefully induces interfacial outflow from emulsion layers to respective continuous phases. These results have been optimally analysed for a duration of 400 seconds. D1 commercial demulsifier, as alighted in Table (4.1) have been used as an illustrative basis for this investigation (i.e. $Z = 1.43 \times 10^{-6}\ mol/m^2$)

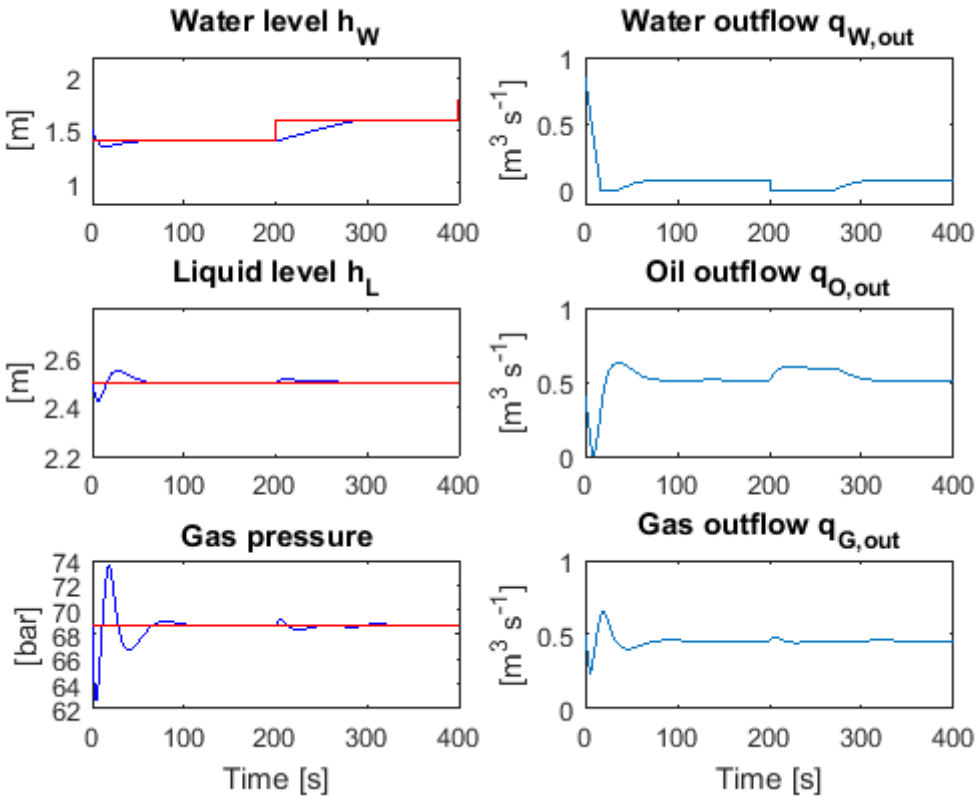

Figure 9. 6. Relationship of fluid outflow with respect to their set level or pressure-Part (1b)

The results from Figure (9.6), shows the level of water, h_W, level of liquid, h_L, pressure of gas and gas outflow, $q_{G,out}$ are controlled to constant level and flowrate as expected. Since the water and liquid level are controlled to a constant level, the water, $q_{W,out}$ and oil, $q_{W,out}$ outflows are consequentially controlled as shown in subplot (3,2,2) and (3,2,4).

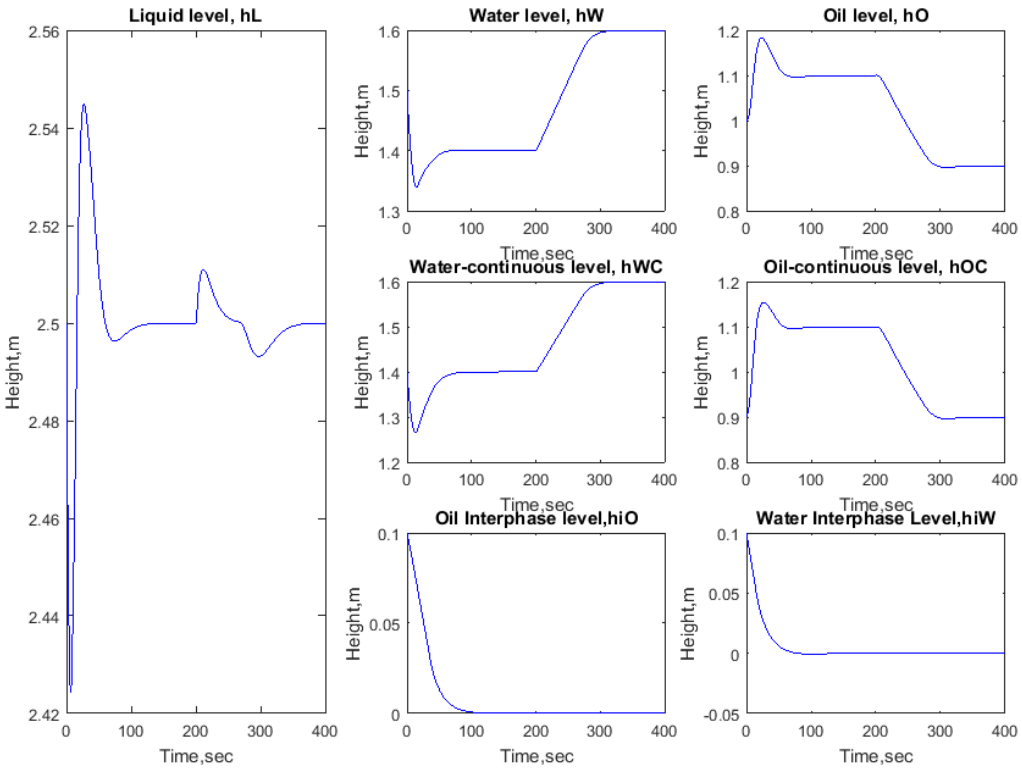

Figure 9. 7. Levels of various composition of the liquid phase with respect to time-Part (1b)

The result of particular interest in Figure (9.7) is subplot (3,3,8) and (3,3,9) (i.e. plot for h_{iO} and h_{iW}), and as shown, the control of oil, h_{iO} and water, h_{iW} interface level via the use of demulsifier is shown to be very effective. This is because the levels of these interfaces were controlled to a set level of zero, desired for effective separation of water and oil. However, the controller for water interface level, h_{iW} seems faster in bringing the level to zero at approximately 80 seconds, as opposed to approximately 95 seconds for the control of the oil interface level, h_{iO}. Furthermore, subplot (1,3,1), subplot (3,3,2) and subplot (3,3,3) validate, $h_L = h_W + h_O$, subplot (3,3,2), subplot (3,3,5) and subplot (3,3,8) also validate, $h_W = h_{WC} + h_{iO}$ and finally subplot (3,3,3), subplot (3,3,6) and subplot (3,3,9) validate that, $h_O = h_{OC} + h_{iW}$.

In reference to Figure (9.8), subplot (2,2,1) and (2,2,2), at initial time of separation, inflowing water and oil streams enter the separator at high turbulence. This enhances a growing emulsion layer, from an initialized value of 0.1 m for both oil and water emulsion layers (i.e. $h_{iW,init} = 0.1m \; and \; h_{iO,init} = 0.1m$). Growing interface layers imply dirtier water and oil phases, which means that the oil-water interfacial tension increases towards its maximum value of approximately $31 - 35 \times 10^{-3} N/m$ for most crude oil emulsions. Because the controller for the interface layer is designed in a feedback configuration, the controller responds by attempting to bring the interface to the desired level as fast as possible. This is achieved via demulsification, through reduction of interfacial tension of the

interfaces to the lowest possible value of $0.005\ N/m$. The demulsifier destabilizes the molecular interaction between the oil and water phase, to enhance higher outflow of water and oil continuous phase from the interface. However, as the controller attempts to destabilize the interface, more water and oil phases, continuously fed to the separator at high turbulence, continue to interact and increase the interfacial tension a little bit. The phenomenon of the controller attempting to reduce the interfacial tension, and inflowing water and oil attempting to increase the interfacial tension, continues and counteract each other. This continues until an optimal interfacial tension is attained that set the oil and water emulsion layer to zero. Observation of result shows that the interfacial tension required to attained the desired interface level of zero is approximately $0.03023\ N/m$ and $0.01613\ N/m$ for water and oil interface layer respectively.

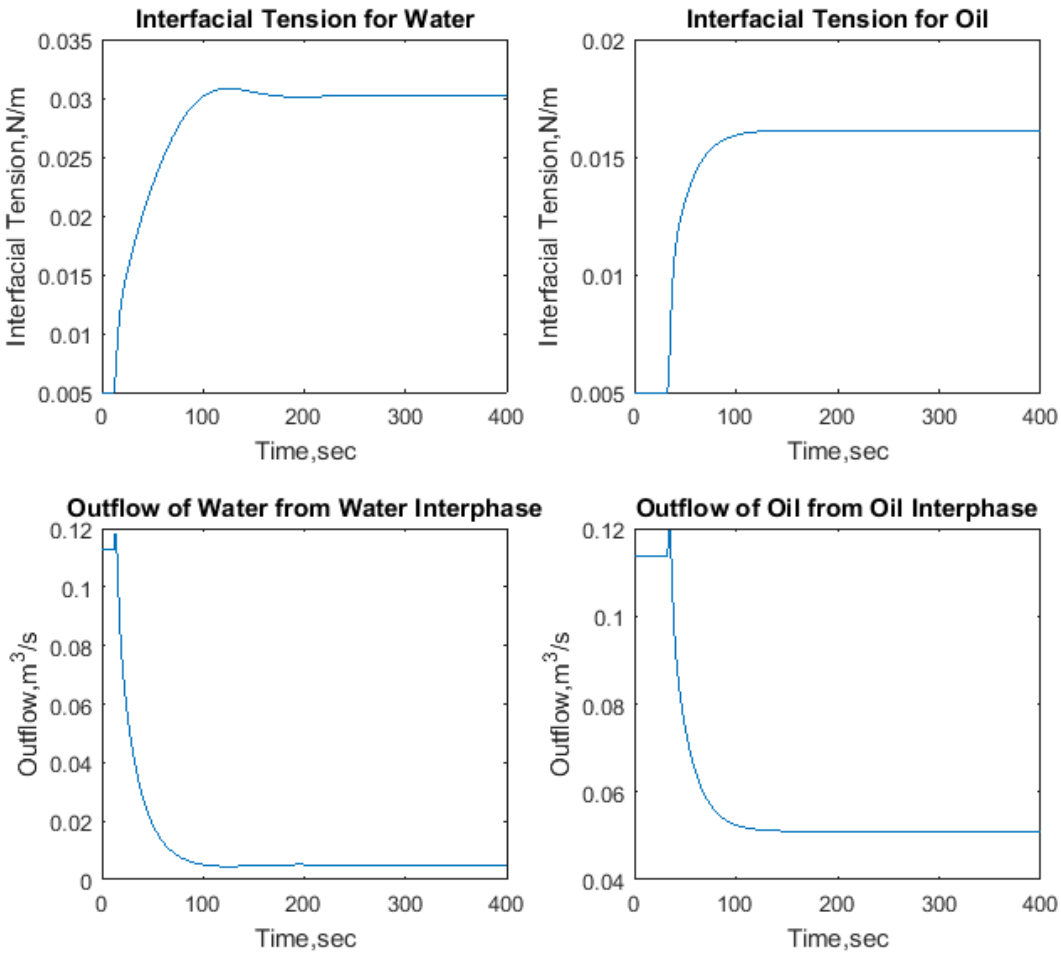

Figure 9. 8. Set interfacial tension and corresponding outflow of demulsified interface layer-Part (1)

Figure (9.8), subplot (2,2,3) and (2,2,4), shows the estimated outflow of water and oil continuous phase from the emulsion layer that corresponds to the prevailing interfacial tension in the separator. The initial interfacial tension of $0.005\ N/m$ for water interface correspond to an outflow of $0.1128 m^3/s$ to the water continuous phase, while at $0.03023\ N/m$ the outflow is $0.0050 m^3/s$. Furthermore, initial interfacial tension of $0.005\ N/m$ for oil interface correspond to an outflow of $0.1138 m^3/s$ to

the oil continuous phase, while at $0.01613\ N/m$ the outflow is $0.0510 m^3/s$. In summary this suggests, lower interfacial tension corresponds to higher outflow from the emulsion layer and vice versa. This is indirectly and directly demonstrated in Figure (9.8) and Figure (9.9), respectively.

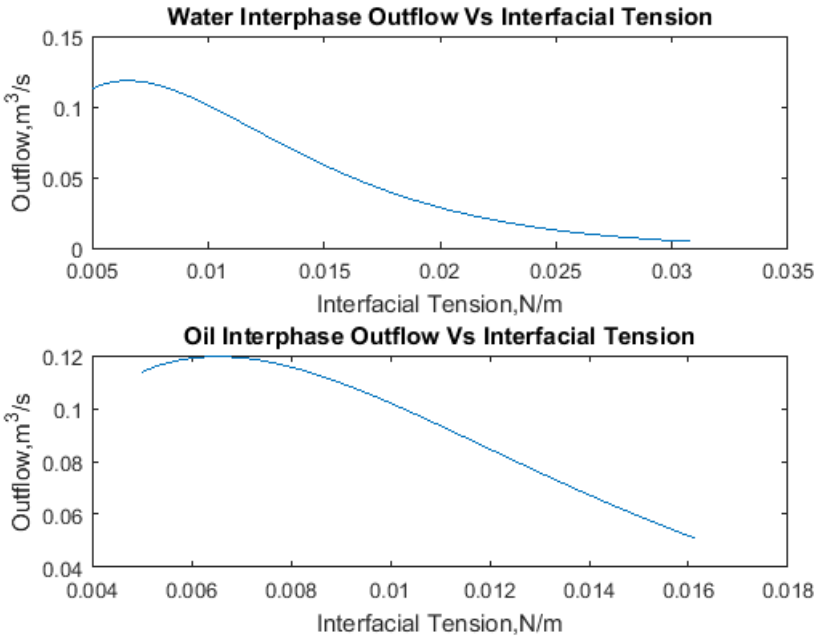

Figure 9. 9. Relationship between outflow from interface and interfacial tension-Part (1)

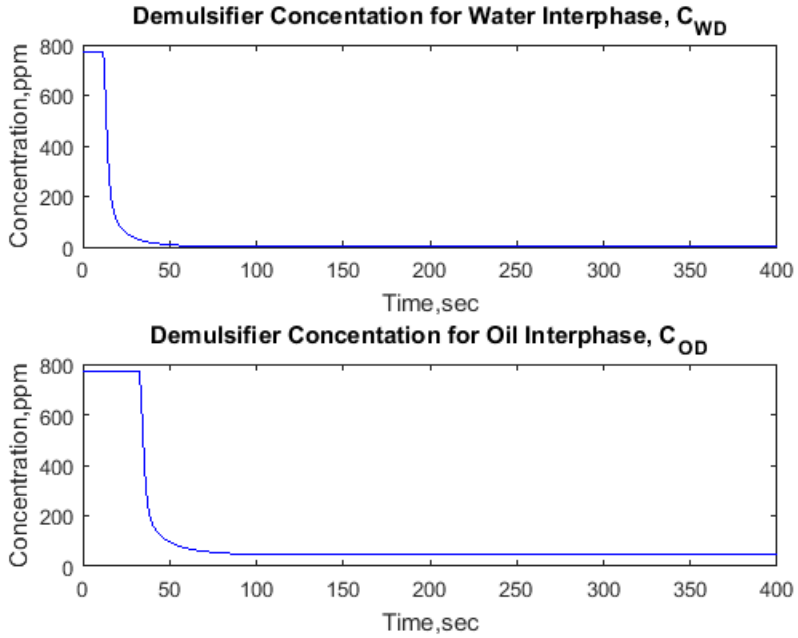

Figure 9. 10. Concentration of demulsifier feed to the separator on batch basis overtime-Part (1)

In reference to Figure (9.10), subplot (2,1,1), at the initial stage of separation, the controller calculated interfacial tension of $0.005\ N/m$ for water interface, is sent to an actuator that delivers an equivalent demulsifier concentration of $774\ ppm$ over a period of 11 seconds. Subsequently, in the next 88 seconds the concentration is controlled to approximately $1.237\ ppm$. Finally, this concentration ($1.237\ ppm$) is maintained over the next 300 seconds of the process.

Similar analysis of Figure (9.10), subplot (2,1,2), show that at the initial stage of separation, the an equivalent of $774\ ppm$ of demulsifier required over a period of approximately 32 seconds. Subsequently, in the next 118 seconds the concentration is controlled to approximately $44.8\ ppm$. Finally, this concentration ($44.8\ ppm$) is maintained over the next 250 seconds of the process.

The above analysis of demulsifier concentration required in this process, have been evaluated on a batch basis and not for a continuous basis. However, the result suggests that more demulsifier are used in demulsification of oil interface as observed in the final stage of the process ($44.8\ ppm$ for oil interface as opposed to $1.237\ ppm$ for water interface). This is of course expected for the oil interface because it's final interfacial tension is smaller ($0.01613\ N/m$) compared to that of water interface ($0.03023\ N/m$). Therefore, this suggest that as concentration of demulsifier increases interfacial tension decreases, as shown in Figure (9.11).

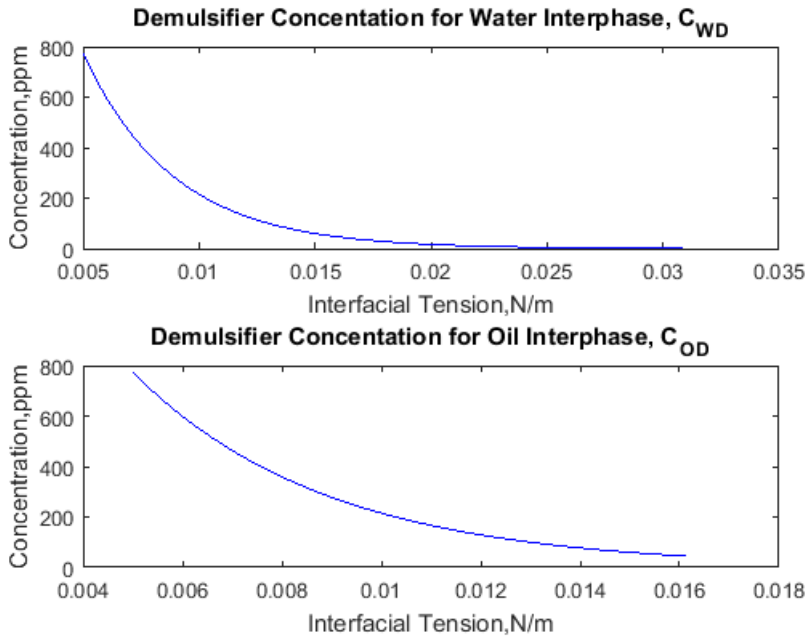

Figure 9. 11. Relationship between concentration of demulsifier and interfacial tension -Part (1)

9.1.3 Conditions with force induced interfacial outflow via flushing

Results shown in Figure (9.12) - (9.13) are deduced for condition when flushing is used to discharge emulsion layers to respective continuous phases. These results have been optimally analysed for a duration of 800 seconds. In deducing these results, an optimal flushing factor, K_{flu} has been deduced as 0.08 and 0.25 for water and oil interface layers, respectively. These optimal values are chosen, based on conditions necessary for flushing, discussed earlier and also based on the magnitude of disturbance in control signals.

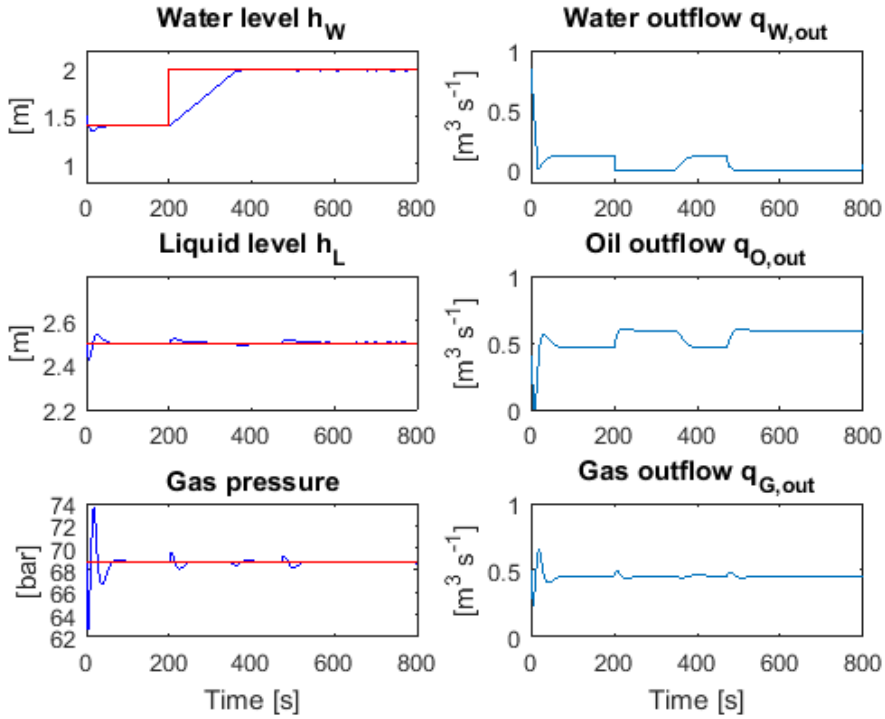

Figure 9. 12. Relationship of fluid outflow with respect to their set level or pressure-Part (1c)

The results from Figure (9.12), shows that level of water, h_W, level of liquid, h_L, pressure of gas and gas outflow, $q_{G,out}$ are controlled to constant level and flowrate as expected. Since the water and liquid level are controlled to a constant level, the water, $q_{W,out}$ and oil, $q_{W,out}$ outflows are consequently controlled as shown in subplot (3,2,2) and (3,2,4). These results are similar to other subcases discussed earlier, the only difference being more alteration in the control signals.

Figure (9.13), subplot (3,3,8) and (3,3,9) shows that, drainage of the oil and water interfaces via flushing is effective. Based on the analysis of Figure (3.1), complete drainage of water interface is expected to be achieved before the drainage of oil interface begins. This process is well illustrated in the results, as complete drainage of water interface is achieved after about 468 seconds, which also marks the beginning of oil interface drainage, shown to have been completed at the end of the simulation, i.e. after 800 seconds. Furthermore subplot (1,3,1), subplot (3,3,2) and subplot (3,3,3) also validate, $h_L = h_W + h_O$, subplot (3,3,2), subplot (3,3,5) and subplot (3,3,8) validate, $h_W = h_{WC} + h_{iO}$, likewise subplot (3,3,3), subplot (3,3,6) and subplot (3,3,9) validate , $h_O = h_{OC} + h_{iW}$.

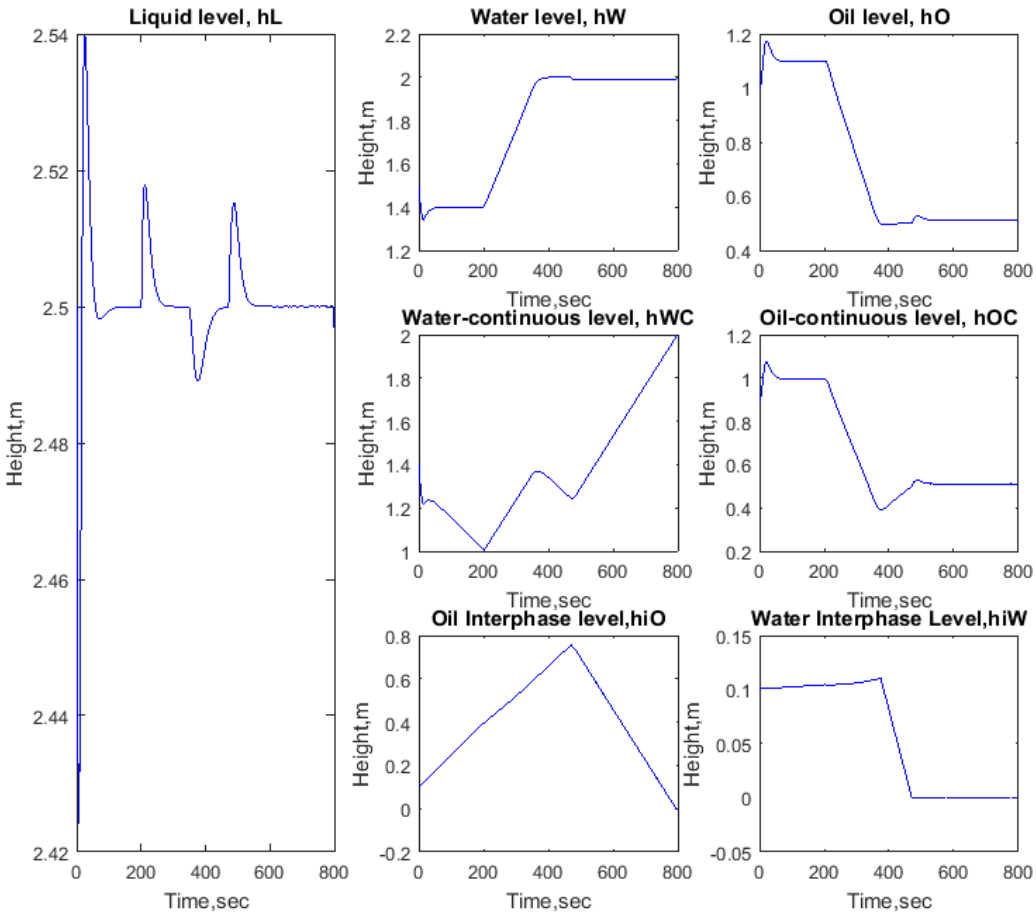

Figure 9. 13. Levels of various composition of the liquid phase with respect to time-Part (1c)

Chapter 9

9.2 Simulation of gravity separator toward the end of reservoir lifetime

Towards the end of the reservoir lifetime, the oil cut in the flow stream entering the separator is at its lowest, and data for this regime are given in Table (9.4).

Table 9. 4.Data for simulation towards the end of reservoir lifetime

Parameters	Description	Value	Unit
α	Water Cut	0.475	–
β	Oil Cut	0.525	–
q_{Lin}	Inlet Volumetric Flowrate of Liquid	0.73	m^3/s
q_{Gin}	Inlet Volumetric Flowrate of Gas	0.456	m^3/s

9.2.1 Conditions with no force induced interfacial outflow

Results shown in Figure (9.14) - (9.18) are deduced for condition when there is no forced induced interfacial outflow from emulsion layers to respective continuous phases. These results have been optimally analysed for a duration of 400 seconds.

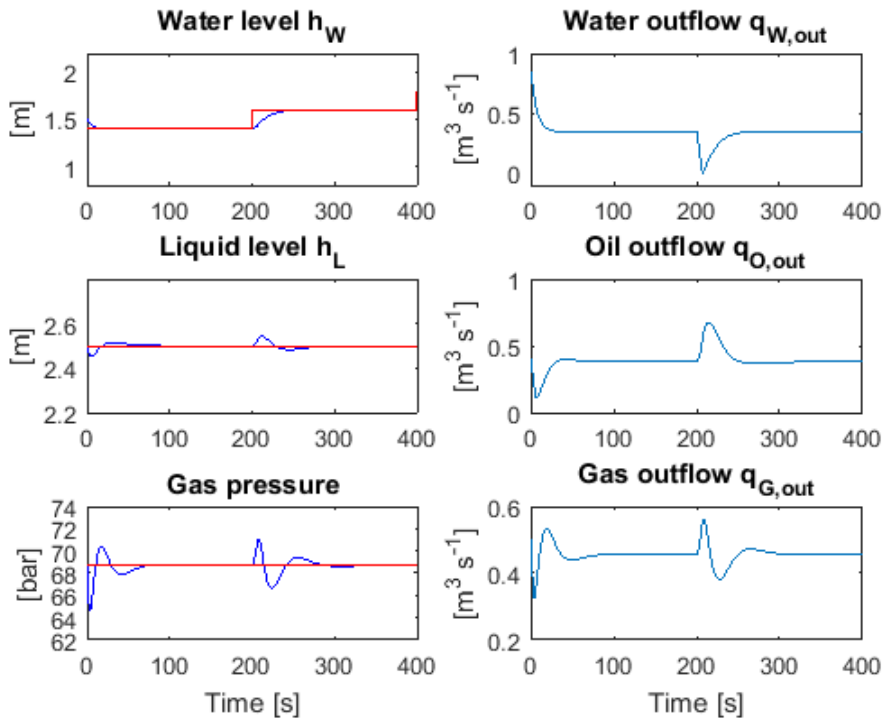

Figure 9. 14. Relationship of fluid outflow with respect to their set level or pressure-Part (2a)

The results in Figure (9.14) is similar to that in Figure (9.1). As expected the water and liquid level are controlled to a constant level, and as such the equivalent water, $q_{W,out}$ and oil, $q_{W,out}$ outflows are discharged from the system.

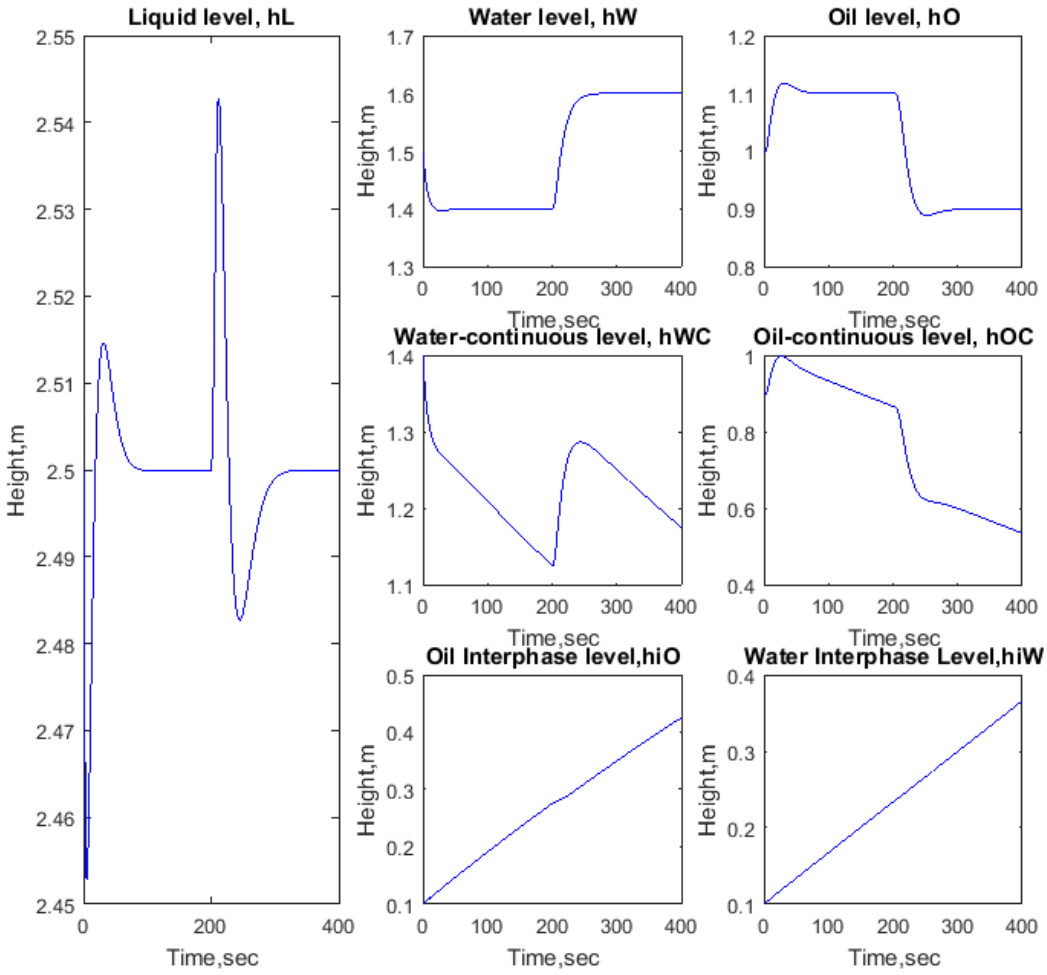

Figure 9. 15. Levels of various composition of the liquid phase with respect to time-Part (2a)

Like previous results, $h_L = h_W + h_O$, $h_W = h_{WC} + h_{iO}$ and, $h_O = h_{OC} + h_{iW}$ are validated in Figure (9.15). Further analysis, shows that comparison to Figure (9.2) subplot (3,3,8) and (3,3,9), also indicates increase in oil, h_{iO} and water, h_{iW} interface level as expected. However, in numerical comparison the growth of oil interface is slightly slower in Figure (9.15) (i.e. 0.1m to 0.4252m as compared to 0.1m to 0.6725m previously in Figure (9.2)). Further comparison shows water interface grows faster as shown in Figure (9.15) (i.e. 0.1m to 0.3643m as compared to 0.1m to 0.1076m previously in Figure (9.2)). This is expected, because the oil cut is lower in this case study (compare Table (9.4) and (9.3)), hence lesser amount of oil is dispersed in the water phase. Furthermore, the water cut is higher (again, compare Table (9.4) and (9.3)), hence more water will be dispersed in the oil phase.

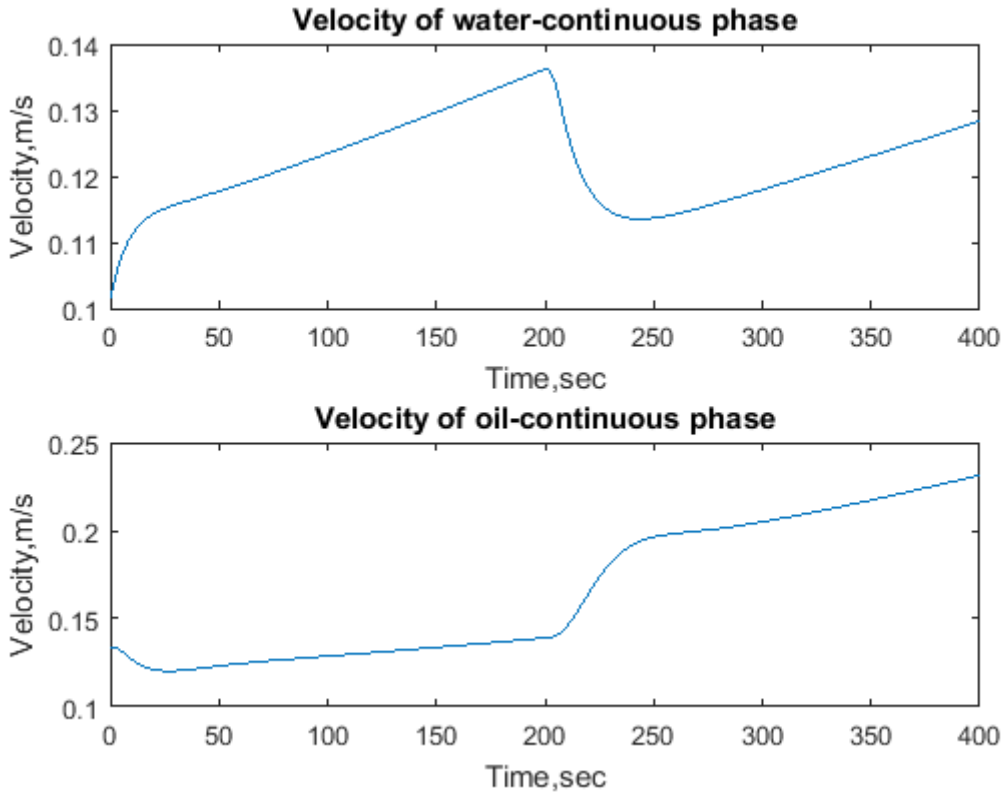

Figure 9. 16. Velocity profile for continuous phases-Part (2)

The analysis of this result is based on previous concluded reasons, that as the respective interfaces grows, velocities of the continuous phases will increase.

Figure (9.16) shows that the velocities for water and oil continuous phases increase with time, just as the previous result shown in Figure (9.3). However, in comparison to previous case shown in Figure (9.3), the oil velocity is higher in this case ($0.23\ m/s$ as compared to $0.19\ m/s$ previously). Similarly, the water velocity is also higher in this case ($0.129\ m/s$ as compared to $0.062\ m/s$ previously). The reason for an increase in the oil phase velocity, is due to more rapid increase in water interface layer (h_{iW} is higher in this case Figure (9.16), subplot (3,3,9) compared to previous case Figure (9.2), subplot (3,3,9)). However, h_{iO} is lower in this case, Figure 9.13, subplot (3,3,9) compared to previous case, Figure (9.2), subplot (3,3,9). Therefore, one would expect that the velocity will be lower in this case, but this is not the case. This is an indication of the fact that the system must act to ensure that the liquid level is kept constant, i.e. $h_L = h_W + h_O$.

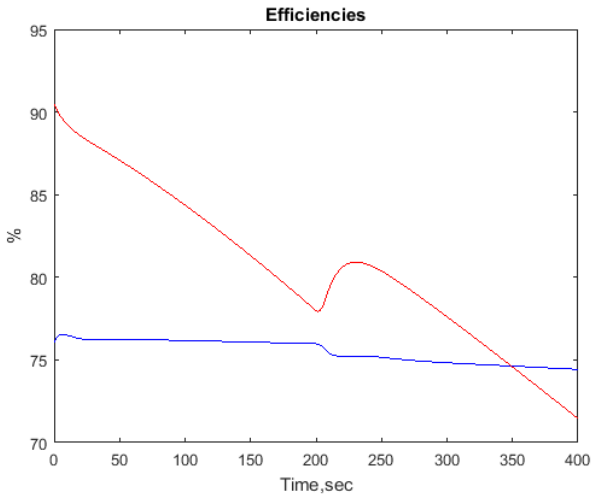

Figure 9. 17. Efficiencies of removal of oil from water (red) and water from oil (blue) over time- Part (2)

Comparing Figure (9.17) to Figure (9.4), shows that the efficiency of oil phase drops from 90.38% to 71.48%, Figure (9.17) compared to previous case that was from 100% to 94%, Figure (9.4). This observable difference in efficiency is due to the increase in water cut in the ending phase of the reservoir (i.e. 0.475 water cut at the end compared to 0.135 cut at the beginning of the reservoir). Furthermore, while the separation efficiency of water phase is approximately constant at 63%, due to very high oil cut at the beginning of reservoir production, there is a difference in efficiency from 76.34% to 74.44%. Water efficiency is obvious higher (74.44% >63%) in this case since the oil cut in the reservoir has reduced from its previous value of 0.865 at the beginning to 0.525 towards the end of the reservoir lifetime. Further illustration of these results is elaborated in Figure (9.18).

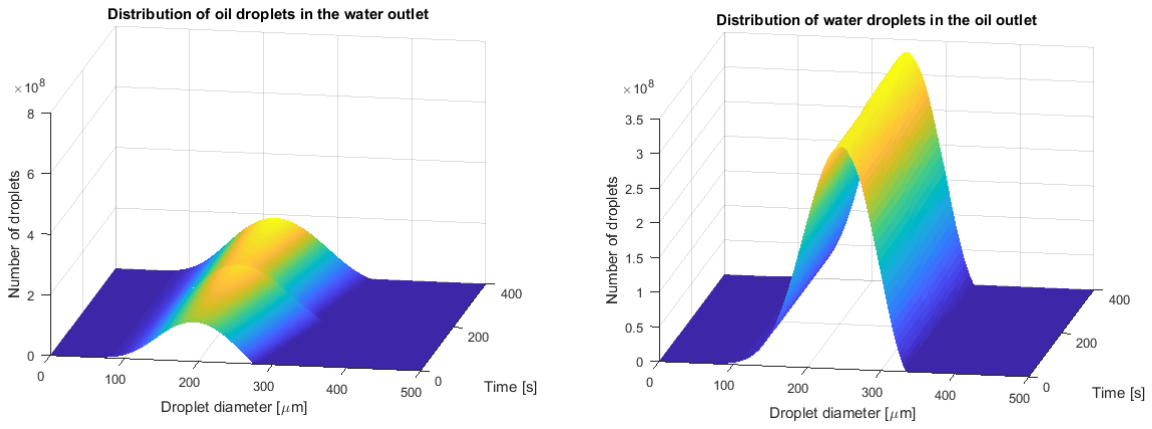

i. Distribution of oil droplets in the water Outlet ii. Distribution of water droplets in the oil outlet

Figure 9. 18. Distribution of disperse phase in continuous phase-Part (1)

9.2.2 Conditions with force induced interfacial outflow via demulsifier

Results shown in Figure (9.19) - (9.24) are for time regime towards the end of reservoir lifetime, deduced for condition when demulsifier forcefully induce interfacial outflow from the emulsion layers to the respective continuous phases.

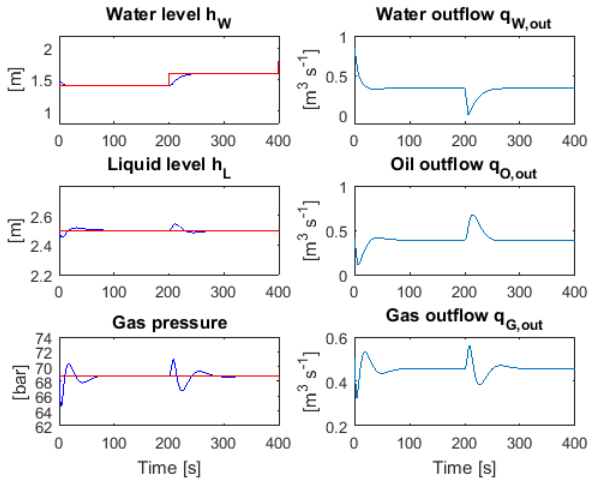

Figure 9. 19. Relationship of fluid outflow with respect to their set level or pressure-Part (2b)

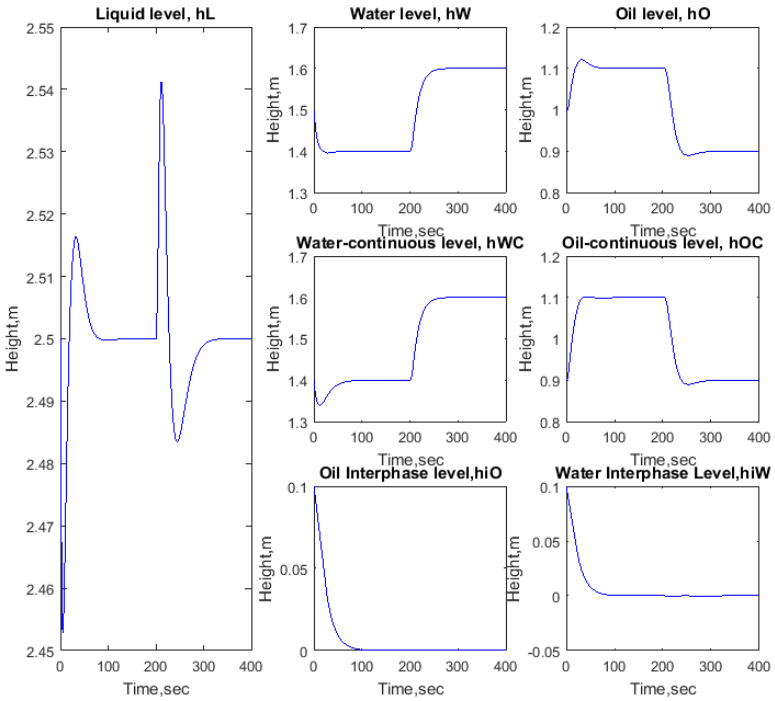

Figure 9. 20. Levels of various composition of the liquid phase with respect to time-Part (2b)

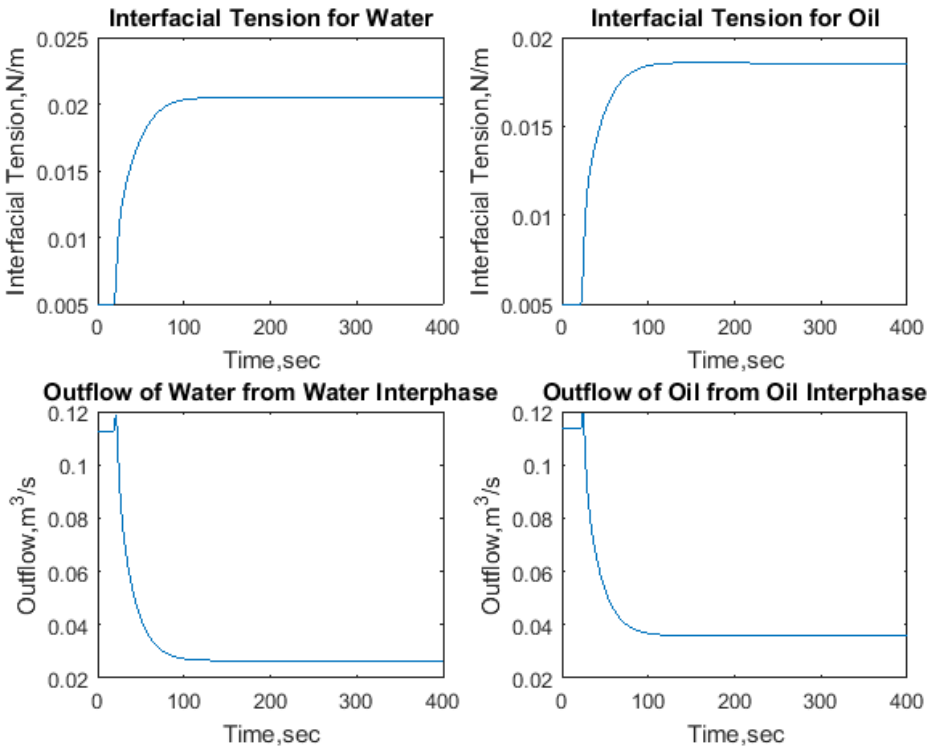

Figure 9. 21. Set interfacial tension and corresponding outflow of demulsified interface layer-Part (2)

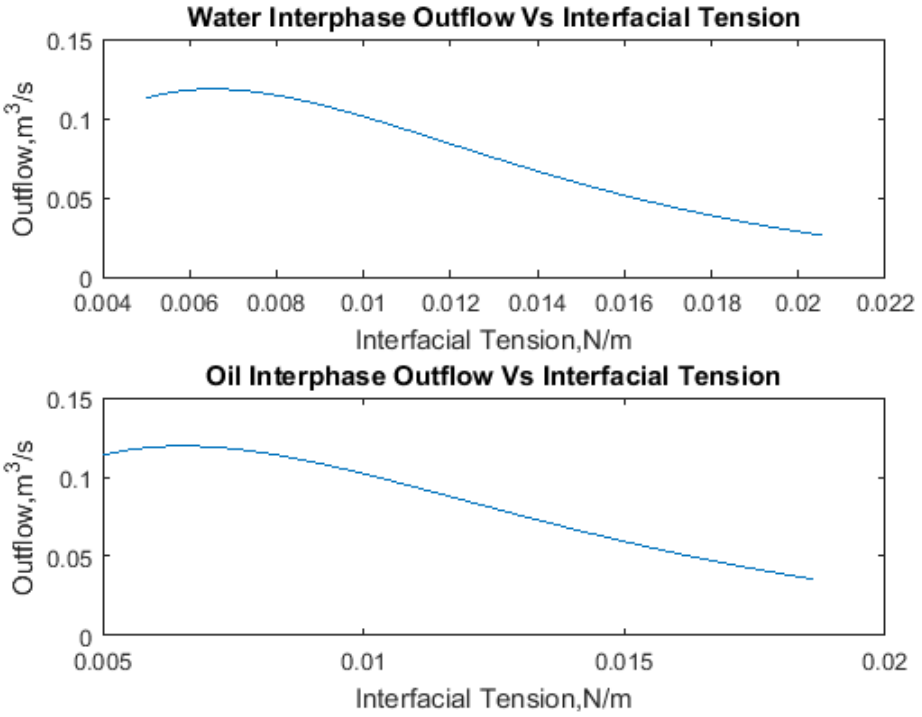

Figure 9. 22. Relationship between outflow from interface and interfacial tension-Part (2)

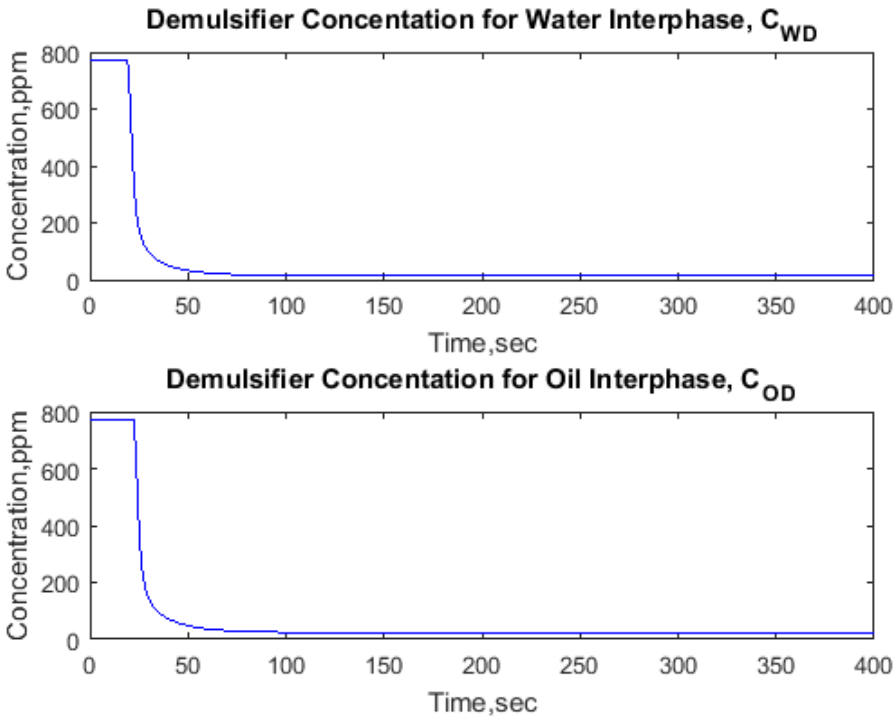

Figure 9. 23. Concentration of demulsifier feed to the separator on batch basis overtime-Part (2)

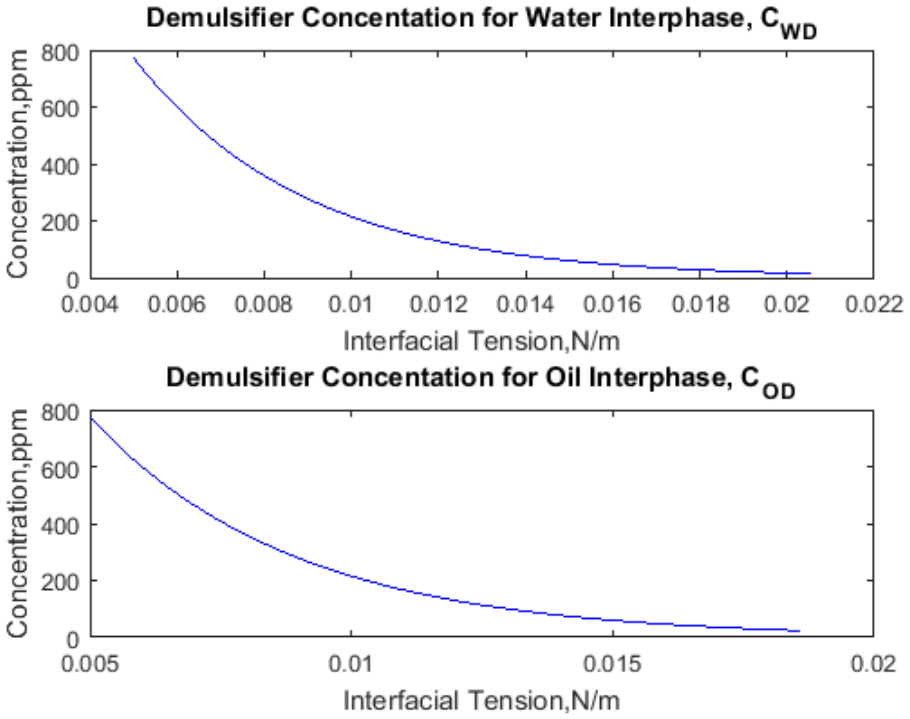

Figure 9. 24. Relationship between concentration of demulsifier and interfacial tension -Part (2)

The results in Figure (9.19) - (9.24) show similar progression as the results in Figure (9.6) - (9.12), the most significant difference is the final values of interfacial tension for the oil interface ($0.01854\ N/m$, Figure (9.21), subplot (2,2,2)) and for the water interface ($0.02052\ N/m$,Figure (9.21), subplot (2,2,1)). These values are different from those obtained in the previous case; $0.01613\ N/m$ for oil and $0.03023\ N/m$ for water interface. Consequently, the resulting outflow from the interfaces are $0.0361\ m^3/s$ for oil interface (as opposed to $0.0510\ m^3/s$ in the previous case) and $0.0264\ m^3/s$ for water interface (compared to $0.0050 m^3/s$ in the previous case). Furthermore, comparison of Figure (9.23) to Figure (9.10) shows similar conclusion, since more demulsifier is required in demulsification of oil interface as observed in the final stage of the process ($24\ ppm$ for oil interface as opposed to $15.4\ ppm$ for water interface)

9.2.3 Conditions with force induced interfacial outflow via flushing

Results shown in Figure (9.25) - (9.26) are for condition when flushing is used to discharge emulsion layers to respective continuous phases. These results were deduced for an optimal duration of 600 seconds and for optimal flushing factor, K_{flu} of 0.26 and 0.4 for water and oil interface layer respectively.

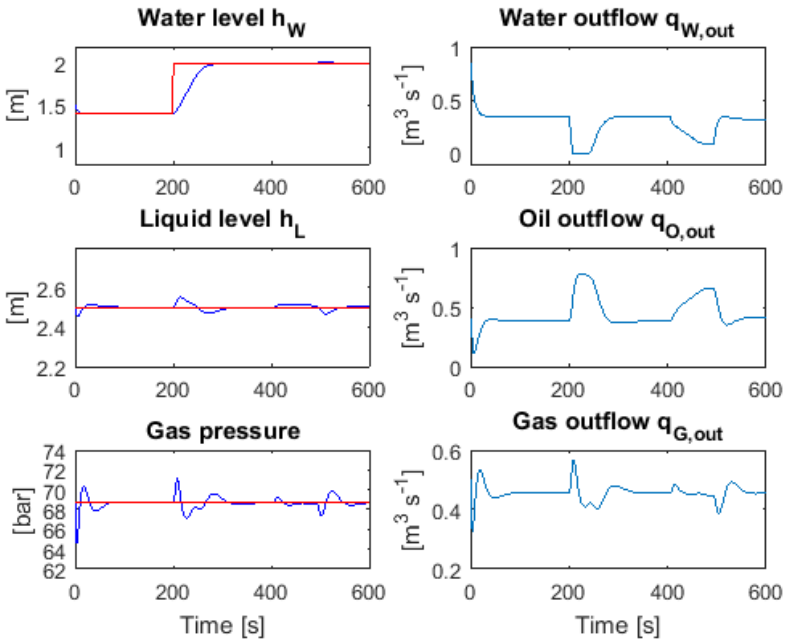

Figure 9. 25. Relationship of fluid outflow with respect to their set level or pressure-Part (2c)

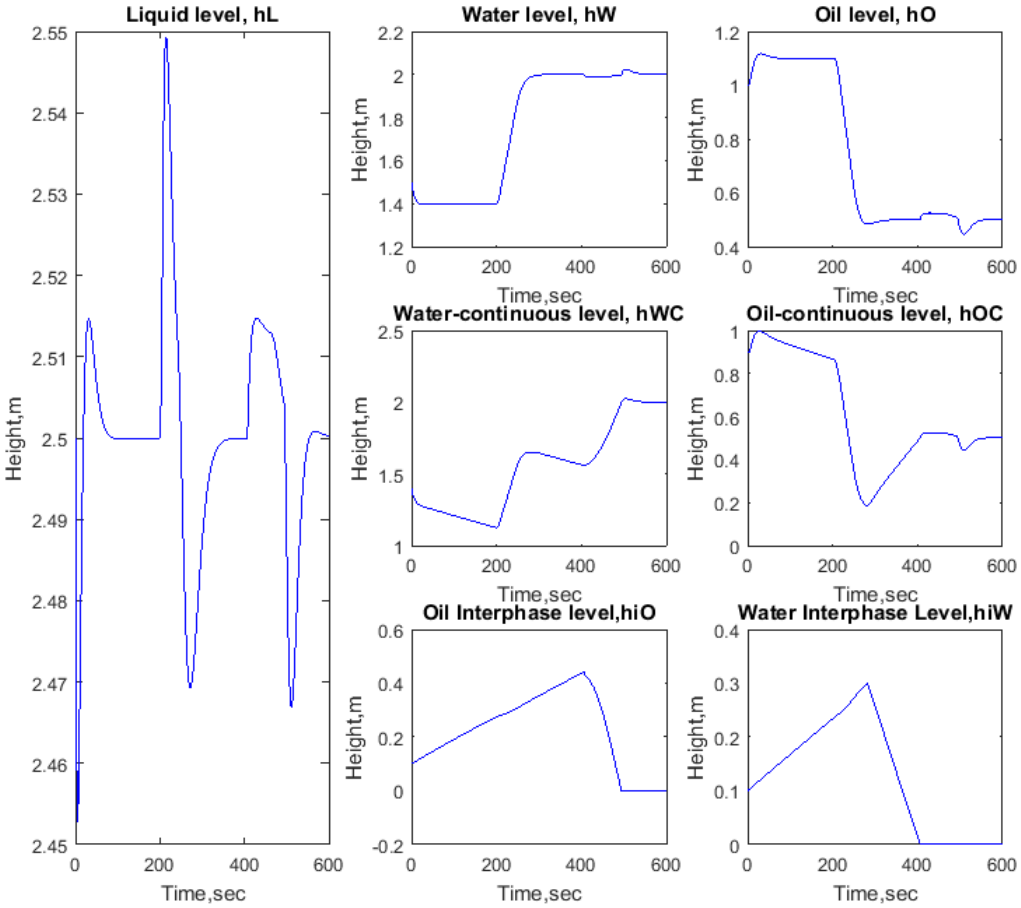

Figure 9. 26. Levels of various composition of the liquid phase with respect to time-Part (2c)

The results in Figure (9.25) -(9.26) have similar progression as the results in Figure (9.11) -(9.12). However, observation differences are in the durations for complete drainage of emulsion layers. Complete drainage of water interface is achieved after about 400 seconds (as opposed to 468 seconds in the previous case), and this time also marks the beginning of oil interface drainage, shown to have been completed after 496 seconds (as compared to 800 seconds from the case before).

Chapter 10

10 Conclusion

The results discussed in chapter 9, validate the assumptions on which the models were developed. The progression of results in each subsection (i.e. unforced, demulsification and flushing of emulsion layer) are approximately similar for the respective cases during well production at the beginning of reservoir lifetime and towards it's end.

Analysis of result in Figure (9.2) and Figure (9.15), subplot (3,3,8) -(3,3,9) for condition when there is no force induced interfacial outflow from emulsion layers, shows that the emulsion layer will continue to grow, and the magnitude of growth is significantly dependent on the respective oil and water cut in the feed stream to the separation.

Results from Figure (9.7) and Figure (9.20), subplot (3,3,8) -(3,3,9) for condition when there is forced induced interfacial outflow via demulsification of the emulsion layers, show that the demulsifier enhance control is effective, as the emulsion layers are completely demulsified to zero. The principle basis of control can be concluded to depend on the interfacial tension. It can be inferred that as interfacial tension decreases, the water and oil interface layers diminish, Figure (9.9) and Figure (9.22). Furthermore, the concentration of demulsifier increases with decrease in interfacial tension, Figure (9.11) and Figure (9.24). In addition, it can be inferred that the demulsification controllers are versatile, as the tuning parameters deduced at the period approaching the end of reservoir lifetime were also found effective for the case representing the beginning of the reservoir lifetime.

Results from Figure (9.13) and Figure (9.26), subplot (3,3,8) -(3,3,9) for condition when there is forced induced interfacial outflow via flushing show that flushing significantly depends on the chosen flushing factors and time. It can also be inferred that the magnitudes of water and oil cuts determine the flushing factors and the duration of flushing. Furthermore, it can be inferred that the process of flushing is adequately modelled based on the analysis in Figure (3.1): Complete drainage of water interface is expected to be achieved before the drainage of oil interface begins.

In conclusion, the emulsification models developed (Equation (3.1)- (3.7)) in this work, can be inferred to be simple and adequate enough to describe the growth of liquid emulsion layers in horizontal gravity separators and as such the performance of separation can be investigated, Figure (9.6)- (9.11) and Figure (9.19)- (9.24). Also, the thermodynamic equation, in collaboration with a curve fitted equation developed for retarded Hamaker constant, is adequate in modelling demulsification of the emulsion layers (Equation (4.3) -(4.4) and (5.1))

Chapter 11

11 Recommendation for Future work

The models developed are adequate to describe liquid emulsification and demulsification in a horizontal gravity separator. Comparison of simulation results, however, have not been undertaken with real measurements from an existing separation unit, hence the robustness of simulation results has not been evaluated.

The values and pairing for interfacial tension, γ, and retarded Hamaker constant, Ha, used in the equations proposed by Grimes, 2012 to model demulsification were deduced on the basis of theoretical evaluation. However, evaluation of these values via experimental investigation would give a more realistic value. Also, the use of experimentally deduced oil and water droplet size distributions in the interface would further enhance the reliability of the simulation result. Based on these facts, I propose a future work to investigate experimental values and pairing for interfacial tension, γ, and retarded Hamaker constant, Ha, and subsequently develop a more reliable empirical relationship between them.

12 References

Al-Sabagh, A. M., Kandile, N. G. & El-Din, M. R. N., 2011. Functions of Demulsifiers in the Petroleum Industry. *Separation Science and Technology,* 46(7), p. 1144–1163.

Al-Sabagh, A. M., Kandile, N. G. & El-Din, M. R. N., 2011. Functions of Demulsifiers in the Petroleum Industry. *Separation Science and Technology,* 46(7), p. 1144–1163.

Amani, M. et al., 2017. An Experimental Study on the Application of Ultrasonic Technology for Demulsifying Crude Oil and Water Emulsions. *Journal of Petroleum & Environmental Biotechnology,* 8(3), pp. 2157-7463.

Backi, C. J., Grimes, B. A. & Skogestad, S., 2018. A control- and estimation-oriented gravity separator model for oil and gas applications based upon first principles. *Industrial & Engineering Chemistry Research,* 57(21), p. 7201–7217.

Backi, C. J. & Skogestad, S., 2017a. *A simple dynamic gravity separator model for separation efficiency evaluation incorporating level and pressure control.* s.l., American Control Conference.

Backi, C. J. & Skogestad, S., 2017b. *Virtual inflow monitoring for a three phase gravity separator.* s.l., IEEE Conference on Control Technology and Applications.

Backi, C. J. & Skogestad, S., 2018. Improved inflow estimation for a gravity separator using cascaded and Kalman-like least squares observers. *Computer Aided Chemical Engineering,* Volume 43, pp. 1153-1158.

Bahadori, A., 2014. Natural Gas Processing: Technology and Engineering Design. In: *Gas–Liquid Separators.* Waltham, USA and Oxford, UK: Gulf Professional Publishing, p. 151–222.

Bothamley, M. & Campbell/Petroskills, J., 2013. *Gas/Liquid Separator : Quantifying Separation Performance-Part 1,* s.l.: s.n.

Chaudhury, M. k., 1987. The Hamaker Constant and the Dispersion Force Component. *Journal of Colloid and Interface Science,* 119(1), pp. 174-180.

Devold, H., 2010. *Oil and Gas Production Handbook.* 3rd ed. Oslo: ABB Oil and Gas.

Dorf, R. C. & Bishop, R. H., 2008 . *Modern Control Systems.* 13th ed. s.l.:Prentice Hall.

Elsharkawy, A. M., Al-Sahhaf, T. A. & Fahim, M. A., 2008. Characterization of Asphaltenes and Resins Separated from Water-in-Oil Emulsions. *Petroleum Science and Technology ,* 26(2), pp. 153-169.

Emebu, S., Backi, C. & Skogestad, S., 2017. *Modelling of Horizontal Gravity Separator:Effect of Oil-Water Interface,* Trondheim: NTNU.

Gas Processors Suppliers Association, 2014. *GPSA Engineering Data Book.* 12 ed. Oklahoma: Gas Processors Suppliers Association.

Grimes, B. A., 2012. Population Balance Model for Batch Gravity Separation of Crude Oil and Water Emulsions. Part I: Model Formulation. *Journal of Dispersion Science and Technology,* 33(4), pp. 578-590.

Kang, W. L. et al., 2013. Study on Demulsification of a Demulsifier at Low. *Petroleum Science and Technology,* 31(6), pp. 1532-2459.

References

Kelland, M. A., 2014. *Production Chemicals for the Oil and Gas Industry, Second Edition.* 2nd ed. London: CRC Press .

Kokal, S., SPE & Aramco, S., 2002. *Crude-Oil Emulsions:A State-Of-The-Art Review.* San Antonio, SPE Production & Facilities.

Larson, K., Raghuraman, B. & Wiencek, J., 1994. Electrical and chemical demulsification techniques for microemulsion liquid membranes. *Journal of Membrane Science,* 91(3), pp. 231-248.

Lyons, W., Plisga, G. & BS, 2004. *Standard Handbook of Petroleum and Natural Gas Engineering.* 2nd ed. s.l.:Gulf Professional Publishing.

Manning, F. & Thompson, R., 1995. *Oilfield Processing of Petroleum: Oilfield Processing: Crude Oil (Volume 2).* 2nd ed. s.l.:PennWell Corp..

Mark Bothamley, J. M. C., 2013. *Gas/Liquids Separators: Quantifying Separation Performance-Part 2,* s.l.: s.n.

Meribout, M., Naamany, A. A. & Busaidi, K. A., 2011. *Interface Layers Detection in Oil Field Tanks: A Critical Review.* s.l.:INTECH Open Access Publisher.

Mohammed, T., 2013. *Gravity Separation: A Separation Free of Charge,* s.l.: s.n.

Mokhatab, S., Poe, W. & Mak, J., 2015. *Handbook of Natural Gas Transmission and Processing: Principles and Practices.* 3rd ed. s.l.:Gulf Professional Publishing.

Moshfeghian, M., 2015. *Gas-Liquid Separators Sizing Parameter.* [Online]
Available at: http://www.jmcampbell.com/tip-of-the-month/2015/09/gas-liquid-separators-sizing-parameter/
[Accessed 3 November 2017].

Mostika, Y. S., Karmazin, V. I., Shutov, V. Y. & Grebenyuk, L. Z., 1999. Selection of an Expression for the Hydrodynamic Drag on a Particle in a Magnetic Separator. *Magnetic and Electrical Separation,* 10(1), pp. 45-55.

Nour, A. H., Suliman, A. & Hadow, M. M., 2008. Stabilization Mechanisms of Water-in-Crude Oil Emulsions. *Journal of Applied Sciences,* 8(8), pp. 1571-1575.

Pradilla, D., Ramírez, J., Zanetti, F. & Álvarez, O., 2017. Demulsifier Performance and Dehydration Mechanisms in Colombian Heavy Crude Oil Emulsions. *Energy Fuels,* 31(10), p. 10369–10377.

Silva, F. L. C., Tavares, F. & Cardoso, M. J. E., 2013. THERMODYNAMIC STABILITY OF WATER-IN-OIL EMULSIONS. *BRAZILIAN JOURNAL OF PETROLEUM AND GAS,* 7(1), pp. 001-013.

Simanzhenkov, V. & Idem, R., 2003. *Crude Oil Chemistry.* 1st ed. Boca Raton: CRC Press.

Skogestad, S., 2003. Simple analytic rules for model reduction and PID controller tuning. *Journal of Process Control,* Volume 13, p. 291–309.

Skogestad, S., 2018. *Advance Process Control.* Trondhiem: NTNU.

Skogestad, S. & Grimholt, C., 2011. *The SIMC method for smooth PID controller tuning.* Trondheim: Springer.

References

SPE International, 2015. *Oil demulsification.* [Online]
Available at: http://petrowiki.org/Oil_demulsification#Mixing.2Fagitation
[Accessed 15 April 2018].

Stewart, M. & Arnold, K., 2007. *Surface Production Operations, Volume 1.* 3rd ed. s.l.:Gulf Professional Publishing.

Tadros, T. F., 2013. *Emulsion Formation and Stability.* 1st ed. Weinheim, Germany: Wiley-VCH.

Tanaka, Z. & Iinoya, K., 1970. New Approximate Equation of Drag Coefficient for Spherical Particles. *Journal of Chemical Engineering of Japan,* 3(2), pp. 261-262.

Wang, X. & Economides, M., 2009. *Advanced Natural gas Engineering.* Houston,Texas: Gulf Publishing Company.

WVT Industries, 2014. *DEMULSIFIER Q03.* [Online]
Available at: http://www.wvt.be/en/solutions/demulsifiers/demulsifier-q03
[Accessed 12 April 2018].

13 Appendix

The appendix section is based on previous work (Emebu, et al.,2017). The essence of this section is to show how equations used in chapter three, were deduced.

13.1 Formulation of Area of a Circular Segment

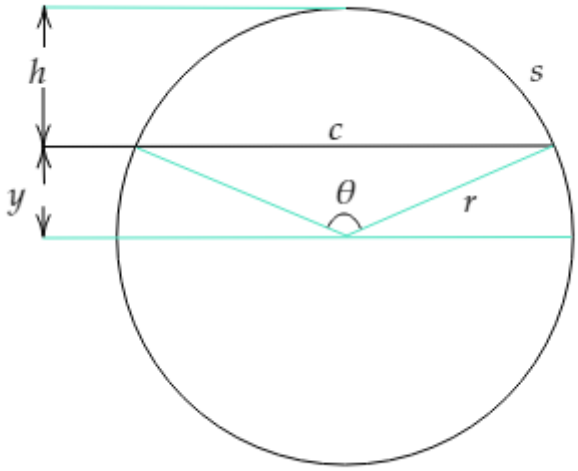

Figure 13. 1. Circle with inscribed segments

As shown in Figure 13.1, is a circle with radius,r, central angle, θ, chord length, c, arc length, s, sagittal height of the segment, h, and height of triangular porton, x.

Given that the sagittal height of the segment, h, and radius of the circle,r is known. Then the arc length, s is given as:

$$s = \theta r$$

Where;

$$\theta = 2\cos^{-1}\frac{r-h}{r}$$

Therefore, area of the circular segment, A, which is equal to the area of the circular sector minus the area of the triangular portion is given as:

$$A = Area\ of\ Circular\ Sector - Area\ of\ Triangle\ Portion$$

Appendix

$$A = \frac{\theta R^2}{2} - \frac{R^2 \sin\theta}{2} = \frac{R^2}{2}(\theta - \sin\theta)$$

Substituting the expression for central angle, θ into the expression for area of circular segment, A.

$$A = \frac{R^2}{2}\left(2\cos^{-1}\left(\frac{r-h}{r}\right) - \sin\left(2\cos^{-1}\frac{r-h}{r}\right)\right)$$

13.2 Derivation for Dynamic Level of Liquid

The essence of this derivation is to show, how the dynamic equation for the liquid phase is deduced. The steps in this derivation is also applicable for derivation of the oil and water phases.

Let, $U = 2cos^{-1}((r - h_L)/r)$ and $V = \sin(2cos^{-1}(r - h_l)/r)$

$$\therefore \frac{dA_L}{dt} = \frac{r^2}{2}\left(\frac{dU}{dt} - \frac{dV}{dt}\right)$$

Differentiating $U = 2cos^{-1}((r - h_L)/r)$, which is same as $(r - h_L)/r = cos\,U/2$ or $1 - h_L/r = cos\,U/2$. Therefore, differentiation of the final expression yields:

$$-\frac{dh_L}{rdt} = -sin\left(\frac{U}{2}\right)\frac{dU}{2dt}$$

Rearranging yields:

$$\frac{dU}{dt} = \frac{2dh_L/dt}{rsin(U/2)} = \frac{2dh_L/dt}{r\sqrt{1 - cos^2(U/2)}} = \frac{2dh_L/dt}{r\sqrt{1 - ((r - h_L)/r)^2}}$$

Differentiating, $V = \sin(2cos^{-1}(r - h_l)/r)$,which is same as $V = \sin y$, and correspondingly where, $y = 2cos^{-1}(r - h_l)/r$, same as $(r - h_L)/r = cos\,y/2$ or $1 - h_L/r = cos\,y/2$.

Differentiating, $V = \sin y$ yields:

Appendix

$$\frac{dV}{dt} = cosy\frac{dy}{dt}$$

Differentiating, $1 - h_L/r = cos\, y/2$ to obtain expression for dy/dt to be substituted into dV/dt

$$\frac{dy}{dt} = \frac{2dh_L/dt}{rsin(y/2)} = \frac{2dh_L/dt}{r\sqrt{1 - cos^2(y/2)}} = \frac{2dh_L/dt}{r\sqrt{1 - ((r - h_L)/r)^2}}$$

$$\therefore \frac{dV}{dt} = cos(2cos^{-1}(r - h_l)/r)\left(\frac{2dh_L/dt}{r\sqrt{1 - ((r - h_L)/r)^2}}\right)$$

Therefore, substituting dU/dt and dV/dt into dA_L/dt yields:

$$\frac{dA_L}{dt} = \frac{r^2}{2}\left(\frac{2dh_L/dt}{r\sqrt{1 - ((r - h_L)/r)^2}} - cos(2cos^{-1}(r - h_l)/r)\left(\frac{2dh_L/dt}{r\sqrt{1 - ((r - h_L)/r)^2}}\right)\right)$$

$$\frac{dA_L}{dt} = \frac{r^2}{2}\frac{2dh_L/dt}{r\sqrt{1 - ((r - h_L)/r)^2}}\left(1 - cos(2cos^{-1}(r - h_l)/r)\right)$$

$$\frac{dA_L}{dt} = r^2\frac{dh_L/dt}{r\sqrt{1 - (r - h_L)^2/r^2}}\left(1 - cos(2cos^{-1}(r - h_l)/r)\right)$$

$$\frac{dA_L}{dt} = r^2\frac{dh_L/dt}{r\frac{\sqrt{r^2 - (r - h_L)^2}}{r}}\left(1 - cos(2cos^{-1}(r - h_l)/r)\right)$$

$$\frac{dA_L}{dt} = r^2\frac{dh_L/dt}{\sqrt{r^2 - r^2 + 2rh_L - h_L^2}}\left(1 - cos(2cos^{-1}(r - h_l)/r)\right)$$

$$\frac{dA_L}{dt} = r^2\frac{dh_L/dt}{\sqrt{h_L(2r - h_L)}}\left(1 - cos(2cos^{-1}(r - h_l)/r)\right)$$

Appendix

The expression for dA_L/dt can be simplified further as follows:

$$\frac{dA_L}{dt} = r^2 \frac{dh_L/dt}{\sqrt{h_L(2r - h_L)}}(1 - cos2\theta)$$

Based on trigonometrical law, $cos2\theta = 2cos^2\theta - 1$, where, $\theta = 2cos^{-1}(r - h_l)/r$, which can be expressed into Figure (13.2) to yield $sin\theta = \sqrt{h_L(2r - h_L)}/r$ and $cos\theta = (r - h_l)/r$.

Therefore $cos2\theta = 2((r - h_l)/r)^2 - 1$. Therefore $1 - cos2\theta = 1 - (2((r - h_l)/r)^2 - 1) = 2(1 - ((r - h_l)/r)^2 = 2(h_L(2r - h_L))/r^2$.

Substituting the expression for $1 - cos2\theta$ into dA_L/dt.

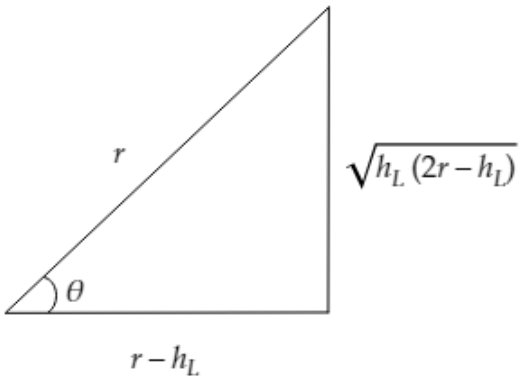

Figure 13. 2. Trigonometrical relationship between, θ , r and $r - h_L$

$$\therefore \frac{dA_L}{dt} = r^2 \frac{dh_L/dt}{\sqrt{h_L(2r - h_L)}} 2(h_L(2r - h_L))/r^2$$

$$\frac{dA_L}{dt} = 2\sqrt{h_L(2r - h_L)}\, dh_L/dt$$

Therefore, substituting the above expression into $dA_L/dt = (dV_L/dt)\,(1/L)$ to derive an expression for dh_L/dt.

$$\frac{dh_L}{dt} = \frac{1}{L}\frac{dV_L}{dt}\frac{1}{2\sqrt{h_L(2r - h_L)}}$$